Penerbit Akademia Baru

Journal of Advanced Research in Experimental Fluid Mechanics and Heat Transfer

http://www.akademiabaru.com/submit/index.php/arefmht
ISSN: 2756-8202

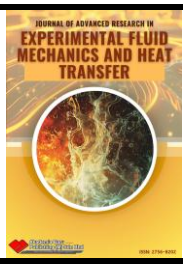

Control of Suddenly Expanded Flow using Quarter Rib for Area Ratio 4.84 at Mach 2

Zakir Ilahi Chaudhary[1], Ambareen Khan[2], Sher Afghan Khan[3,*], Mohammad Nishat Akhtar[4], Khizar Ahmed Pathan[5]

[1] Department of Mechanical Engineering Automobile, M. H. Saboo Siddik College of Engineering, Mumbai, 400008, India
[2] Centre for Instructional Technology and Multimedia, Universiti Sains Malaysia, Pulau Pinang, Malaysia
[3] Department of Mechanical & Aerospace Engineering, Faculty of Engineering, IIUM, Kuala Lumpur, Malaysia
[4] School of Aerospace Engineering, Universiti Sains Malaysia, Penang, 11600, Malaysia
[5] Department of Mechanical Engineering, CSMSS Chh. Shahu College of Engineering, Aurangabad, Maharashtra, India

ABSTRACT

Occurrence of sudden expansion is widespread in the defense and automobile industry. At the blunt base of the fuselage, missiles, projectiles, and aircraft bombs, the flow gets separated at the base and forms low-pressure recirculation, leading to a significant increase in the base drag. This paper addresses how this low base pressure at the base can be controlled. A detailed numerical study was conducted to assess the impact of the quarter circle as a passive control mechanism in a suddenly expanded flow for an area ratio of 4.84 at Mach M = 2.0 for various rib radii ranging from 1 mm to 4 mm, the different duct lengths from L = 1D to 6D at different nozzle pressure ratio ranging from 3 to 11. The findings of this study show that a 1 mm rib is inadequate to impact the flow field inside the duct. Passive control in the form of a quarter circle rib seems to become effective once the nozzle flows under a favorable pressure gradient. However, the remaining rib radii effectively reduce the suction created at the base of the recirculation zone. It is found that the rib radius of 4 mm when placed at 66 mm at the base, results in a maximum rise in the base pressure, and the base pressure ratio attains a value of 3.4. These results are case sensitive; hence, one has to make a final decision about the rib radius, rib location, and the level of expansion based on the end user requirement.

Keywords:
Skin-friction drag; wave drag; base drag; nozzle pressure ratio; L/D ratio

Received: 5 January 2025	Revised: 4 February 2025	Accepted: 7 March 2025	Published: 30 March 2025

1. Introduction

Turbulence has been an enigma since the beginning of fluid science. Since we cannot avoid turbulence in the natural and engineered flows surrounding us, we must understand it. Understanding turbulence is necessary to control the drag associated with turbulent flows. When fluids are mixed or an increase in skin friction drag is required, there are flows where turbulence is desired. In engineering flows, however, turbulence is undesirable and should be controlled to minimize energy input. Significant financial and ecological consequences are linked to turbulent drag in engineering and real-world flows. The use of fossil fuels by various processes in the industry.

* *Corresponding author.*
E-mail address: sakhan@iium.edu.my (Sher Afghan Khan)

https://doi.org/10.37934/arfmts.19.1.129

Flow separation, recirculation, and reattachment are complicated axisymmetric expansion flow field characteristics. Such a flow field can be separated into two main areas by a shear layer: the central flow region and the flow recirculation area. The point where the dividing streamline meets the wall is known as the reattachment line. There is a wealth of information about abrupt expansion issues in the literature. They are, nonetheless, limited to particular flow and geometrical parameter scenarios. If the chapter scans the whole body of literature, it will get very long.

Consequently, this assessment covers the data immediately related to the current inquiry. Wick [1] explored the impact of the boundary layer on sonic flow through an abrupt cross-sectional area. Through experimentation, he found that the kind and thickness of the boundary layer upstream of the expansion determined the pressure in the expansion's corner. He believed that the corner flow's fluid source was the boundary layer. Nevertheless, the boundary layer was also considered insulating air, which lessens the jet's pumping efficiency. The corner at the base was seen as a sump with two bulk supplies. The first source was the boundary layer flow around the corner, and the second was the backflow in the boundary layer along the section's extended wall. The pressure differential across the shock wave that started when the jet hit the wall caused this backflow. He concluded that the internal and exterior flow mechanisms were the same and that studying the base pressure phenomenon in the external flow could be done reasonably fast through internal flow studies.

As far as the authors know, no one has ever tried the quarter rib circle as the control mechanism for base pressure. So far, researchers have used rectangular, semi-circular, triangular ribs. Among all these three ribs, the rectangular rib was most effective in regulating the base pressure as two secondary vortices were created at the two sharp corners of the ribs; later, it was found that the triangular rib was also, but the increase in the base pressure was less as compared to the rectangular ribs. Among them, the semi-circular rib was the least effective as the flow sees a smooth variation in the control shape and does not generate any powerful secondary vortices. This study will fill the research gap as we use passive control in the form of quarter circular ribs at low supersonic Mach numbers. At this Mach number M = 1.3, the base pressure is lower than the ambient pressure, and the contribution from the base drag due to this low base pressure can be around seventy percent of the total drag, which is significant. Therefore, even a slight increase in the base pressure will decrease the aerospace vehicles' base drag and overall drag.

2. Literature Review

In this section, we will scan the literature on the base pressure control in a suddenly expanded flow. There are two methods of control: (i) Passive control and (ii) Active control. Passive control can be accomplished by altering the geometry whenever the active control mechanism is used. It requires an external source of energy, which is very complex if the same is not available through the propulsion system of the aerospace system.

The regulation of base pressure in abruptly expanded flows has emerged as a significant area of scholarly inquiry, primarily because of its essential function in enhancing aerodynamic performance. Pathan *et al.,* [2,3] underscored the necessity of geometric optimization to enhance base flow characteristics. They emphasized that design is not merely a component but a critical factor in augmenting aerodynamic efficiency, particularly in high-speed environments. Similarly, Fiqri *et al.,* [4] and Aqilah *et al.,* [5] illustrated that passive control strategies, including strategically positioned cavities and geometric alterations, facilitate flow reattachment while improving base pressure in sonic Mach number scenarios. Furthermore, duct length and expansion geometry have been shown to influence flow behavior considerably [6]. Pathan *et al.,* [7] investigated duct lengths within expanded flows, discovering that optimized dimensions can substantially reduce pressure losses and

enhance overall performance. Azami *et al.,* [8,9] provided crucial insights into the influence of nozzle configurations on supersonic flow dynamics, demonstrating how such designs shape flow patterns and aid in developing effective passive control techniques.

Similarly, Pathan *et al.,* explored nozzle optimization through variations in wall thickness, highlighting its dual benefits: enhanced performance and reduced structural weight [10]. These findings underscore the potential of passive strategies, such as quarter-circle ribs, to improve flow control significantly. In addition to the active control, the research on passive control mechanisms has shown that features like ribs are highly effective in controlling base pressure and mitigating drag in high-speed aerodynamic configurations [11-22]. Khan *et al.,* [17] demonstrated that quarter and semi-circular ribs improve flow reattachment and reduce base drag in suddenly expanded ducts. These results align with the current study's findings, which indicate that a quarter-circle rib with a radius of 4 mm significantly enhances base pressure when strategically positioned. However, it is essential to consider the broader implications of these configurations because they may lead to advancements in various aerodynamic applications. Although the complexity of these designs can be daunting, this research paves the way for future innovations.

Notwithstanding the progress in this field, significant gaps persist in comprehending the synergistic impacts of various passive control methodologies across a spectrum of parameters [23-29]. Moreover, although most research predominantly emphasizes static geometries, there exists an imperative to investigate adaptive designs that can dynamically respond to fluctuating flow conditions, potentially enhancing aerodynamic performance [30-39]. Addressing these lacunae is crucial because it would propel the development of customized solutions tailored to specific operational criteria, as evidenced by the case-sensitive attributes of rib radii and their placement highlighted in this study.

Rathakrishnan [40] studied the effect of rib in a suddenly expanded flow at sonic Mach numbers. He conducted experiments at various nozzle pressure ratios ranging from 1.141 to 2.54 for 3:1, 3:2, and 3:3 rib aspect ratios. His investigation revealed a decreasing trend in the base pressure at a lower aspect ratio, and control decreases the base pressure. The base pressure increased when an aspect ratio of 3:3 rib was employed. Therefore, depending upon the end user's demands, these combinations of the ribs can be used. If the mission requirement is to increase the base pressure, then the rib with an aspect ratio is ideal. The rib with an aspect ratio of 3:1 is the right choice when the application is in a combustion chamber. In the present study, we have validated our CFD results first with the experimental results of Rathakrishnan [40]. After validation, we took various rib geometry, rib location, and nozzle pressure ratios to study passive control's effect on base pressure.

This body of literature underscores the promise of quarter-circle ribs as efficacious passive control instruments for regulating base pressure and ameliorating flow characteristics, particularly when subjected to particular geometric and operational parameters. These findings elucidate the intricate relationship between duct design and aerodynamic outcomes, particularly pertinent to implementing quarter-circle ribs in regulating suddenly expanded flows at Mach 2. However, these studies show the necessity of continued research in this area, as the interdependencies among various factors remain fully understood. Although promising, this endeavor requires further investigation because the complexities involved are substantial. From the above review, there is evident research on low supersonic Mach numbers. So far, none of the researchers has ever used quarter rib circles to regulate the base flows at sonic and supersonic Mach numbers.

3. Finite Volume Method

3.1 Governing Equations

The following hypotheses are taken into consideration:

i. Turbulent flow is considered because of the turbulent viscous dissipation effects.
ii. The fluid's viscosity varies with temperature and is compressible.
iii. At atmospheric pressure, the flow exits the duct.
iv. While scanning the literature, we found that the internal flow k-epsilon turbulence model is the best as it gives reasonably good results. Khan *et al.,* [17] employed the usual k-epsilon turbulence model to simulate internal flow. As a result, the standard k-epsilon turbulence model is applied to the circumstance. Sutherland's three-coefficient viscosity model is expressed as follows in Eq. (1):

$$\mu' = \mu'_o \left(\frac{T_a}{T_{a,o}}\right)^{3/2} \frac{T_{a,o}+S\prime}{T_a+S\prime} \tag{1}$$

The reference viscosity value in kg/m-s is denoted as μ'_o,, where μ' represents the viscosity. T_a denotes static temperature, K represents the temperature of a standard reference, and S' is the temperature-dependent Sutherland constant. Three-dimensional continuity equation for compressible flow:

The Eq. (2) for mass balance is as follows:

$$\frac{\partial \rho}{\partial t} + \underline{\nabla} \cdot \left(\rho \underline{V}\right) = 0 \tag{2}$$

where the fluid's velocity is denoted by V.

The Eq. (3) for momentum balance is:

$$\frac{\partial}{\partial t}\left(\rho \underline{V}\right) + \underline{\nabla} \cdot \left(\rho \underline{V}\underline{V}\right) + \underline{\nabla} p = \underline{\nabla} \cdot \left[2\mu\left(\underline{\nabla V}\right)_o^s\right] + \underline{\nabla} \cdot \left(\tau_{=Re}\right) \tag{3}$$

where $\left(\underline{\nabla V}\right)_o^s = \left(\underline{\nabla V}\right)^s - \frac{1}{3}\left(\underline{\nabla} \cdot \underline{V}\right)\underline{I}$, $\left(\underline{\nabla V}\right)^s = \frac{\underline{\nabla V} + \underline{\nabla V}^T}{2}$, and $\tau_{=Re}$ is the turbulent stress tensor.

The formulae for Eq. (4) total energy are as follows:

$$\frac{\partial}{\partial t}\left[\rho\left(\frac{1}{2}V^2 + u_{int}\right)\right] + \underline{\nabla}\left[\rho\left(\frac{1}{2}V^2 + u_{int}\right)\underline{V}\right] = \underline{\nabla}\left(\lambda \underline{\nabla} T - p\underline{V} + 2\mu \underline{V} \cdot \left(\underline{\nabla V}\right)_o^s + \underline{V} \cdot \tau_{=Re}\right) \tag{4}$$

where u_{int} is the internal energy, and λ is the thermal conductivity.

Many internal flow simulations use the k-epsilon turbulence model due to its affordability, resilience, and sufficient accuracy. The Ansys Fluent program incorporates the k-epsilon (ε) turbulence model used in this research. The K-equation in Eq. (5) allowed us to calculate the turbulent kinetic energy.

$$\frac{\partial}{\partial t}(\rho k) + \underline{\nabla} \cdot \left(\rho \underline{V} k\right) = \underline{\nabla} \cdot \left[\left(\mu + \frac{\mu_t}{\sigma_k}\right)\left(\underline{\nabla} k\right)\right] - \rho\varepsilon + M_x \tag{5}$$

The turbulent kinetic energy dissipation rate is denoted by ε, the turbulent Prandtl number is σ-k, and the word Mx is the turbulence generation. Precisely, the dissipation (or (-equation)) is controlled by Eq. (6),

$$\frac{\partial(\rho\varepsilon)}{\partial t} = -\underline{\nabla}\cdot\left(\rho\varepsilon\vec{V}\right) + \underline{\nabla}\cdot\left[\left(\mu + \frac{\mu_T}{\sigma_\varepsilon}\right)\nabla\varepsilon\right] - C_1 f_1\left(\frac{\varepsilon}{k}\right)M - C_2 f_2\frac{\varepsilon^2}{k} \quad (6)$$

where $\mu_t = \rho f_\mu C_\mu k^2/\varepsilon$ denotes turbulent viscosity, and the arbitrary constants are denoted as $\overline{C_\mu} = 0.09$, $\overline{C_1} = 1.44$, $\overline{C_2} = 1.92$, $\overline{f_\mu} = 1$, $\sigma_k = 1.0$, and $\sigma_\varepsilon = 1.3$.

3.2 Geometry and Modelling

The finite volume technique (FVM) was employed to delve further into this investigation. The CFD simulation used the ANSYS FLUENT 2024/R2 software to assess the nozzle's fluid flows. We are examining the impact of the quarter geometry of the rib in the form of a passive control method. The orientation of the quarter rib is shown in Figure 1.

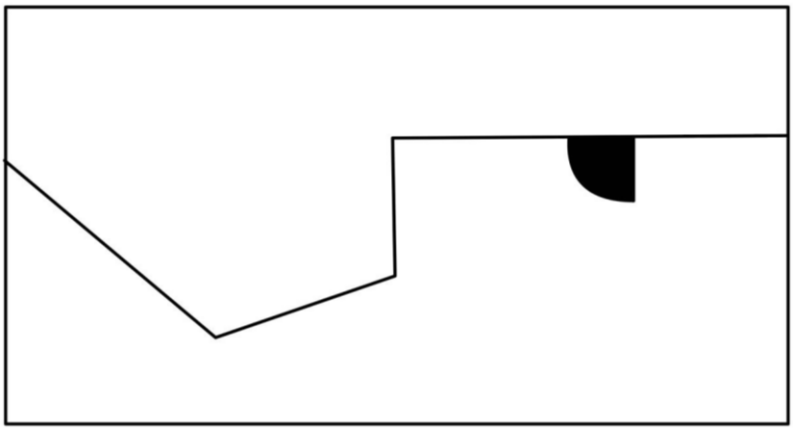

Fig. 1. Orientation of the Rib

3.3 Meshing and Boundary Conditions

A crucial part of the CFD process is meshing. By choosing the free-face mesh type, the 2D model is of the structured mesh type in this case. Elements were given sizes according to each line (edge) length when the constructed structured mesh type was used. The lines were utilized to apply the element size, and elements with identical forms were created using face meshing. The mesh independence check is done. Figure 2 below shows the mesh's element type and size tested during mesh independence check.

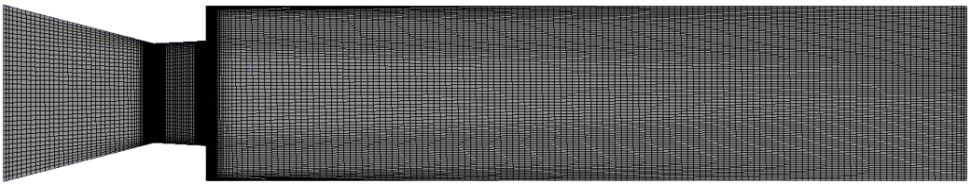

(a)

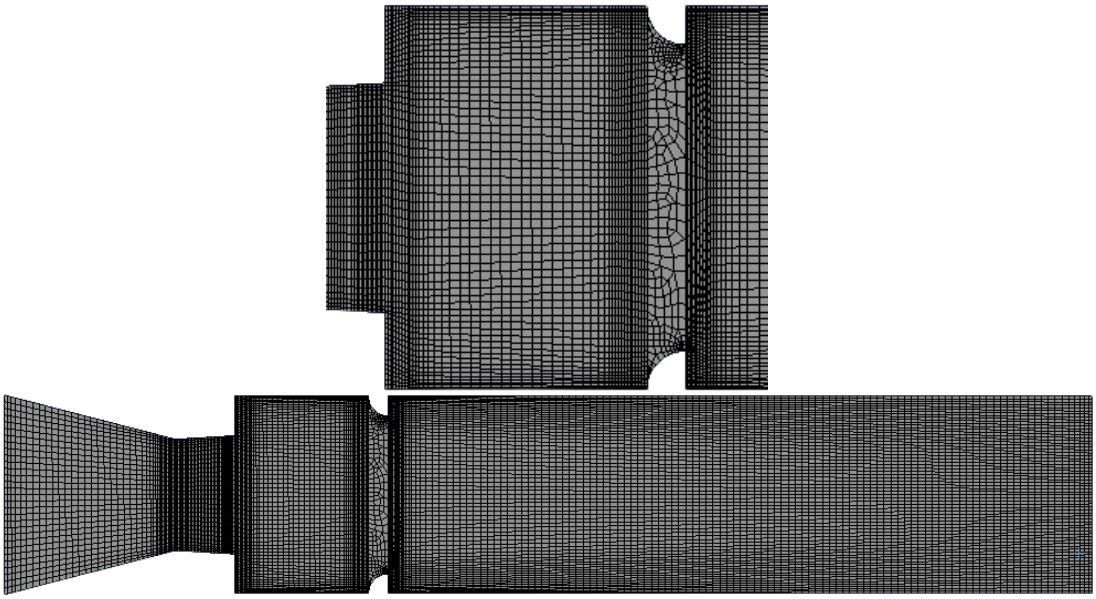

(b)

Fig. 2. Mesh model (a) without ribs (b) with ribs

3.4 Assumptions and Fluid Properties

Assumptions are accomplished to replicate the flow activities in the precise physical environment. Appropriate mathematical and numerical models are selected to make simpler the governing equations.

The governing equations were solved simultaneously; numerical modeling requires choosing the appropriate mathematical models, such as the governing equations, boundary conditions, mesh quality, and numerical method. Despite its limitations in accurately representing physical phenomena, the computational method has been trusted for decades and offers sufficient insight into flow behavior. As a result, this calls for careful consideration of elements that closely resemble the flow behavior. This study pinpoints the presumptions that jeopardize the precise physical state. The following are the presumptions and characteristics covered in this study:

i. The flow is assumed to be a steady 2D flow because geometry is symmetric. Hence, the assumption that the flow is 2-D is justified.
ii. The density of the air is variable as the flow is compressible. The inlet pressure is the gauge pressure at that Mach number and NPR, and at the outlet of the duct, the gauge pressure at the outlet is zero.
iii. Since turbulent flow has a significant impact on turbulent viscous dissipation at a given flow velocity, it is taken into consideration.
iv. The viscosity of the fluid is dependent on temperature.
v. At the standard atmospheric pressure, the flows leave the duct. At normal ambient pressure, the flows leave the duct.

Since the flow via the nozzle is considered turbulent, the compressible flow field is represented by the k-epsilon standard model. The subsequent equations most appropriately characterize the turbulent flow.

3.5 Geometry of the Model

The ANSYS Workbench program utilized fluid flow (Fluent) analytical techniques and was employed for the entire computational fluid dynamics (CFD) procedure. The model was generated via a Design Modeller. Figure 3 depicts a converging nozzle that abruptly widens into a duct with five ribs. In Rathakrishnan's [40] experimental setup, the dimensions of the convergent-divergent nozzle with a suddenly expanded duct are as stated in Table 1.

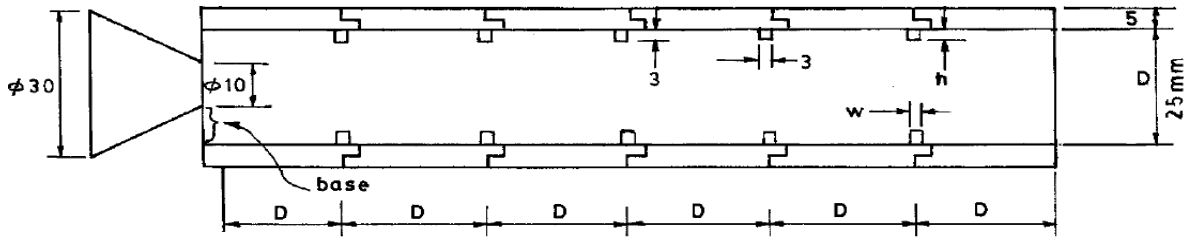

Fig. 3. Duct with five ribs used in an experimental study [40]

Table 1
The geometries of the validation model

Parameters	Dimensions
Nozzle inlet diameter	30 mm
Nozzle outlet diameter	10 mm
Duct diameter	25 mm
Duct length	Varies from 1D to 6D
Converging length	20 mm
Rib width	3 mm
Rib height	Varies from 1mm to 3mm

Table 1 shows the geometrical parameters of the converging nozzle, the duct, and the ribs. As a first step, the CFD results were validated with E. Rathakrishnan's experimental results (39). After validation, a new duct diameter and variations in rib geometry were selected.

3.6 Validation of Previous Work.

According to Rathakrishnan [40], the prior work was performed at aspect ratios of 3:3, 3:2, and 3:1; an area ratio of 6.25; L/D ranging from 1 to 6; pressure ratios of 1.141, 1.295, 1.550, 1.707, and 2.458; and nozzle exit Mach numbers of 0.44, 0.62, 0.82, 0.91, and 1.0. However, in a prior publication by Rathakrishnan [40], the result from Figure 4 with NPR (P_{01}/P_a) 2.458 and models with control in the form of ribs with 3:2 and 3:3 aspect ratios were chosen to be compared to the current work. The simulation is supported by Rathakrishnan's [40] experimental work, which used five ribs positioned at equidistant intervals in the duct, as illustrated in Figure 4. The results of base pressure fluctuation with NPR of 2.458 and L/D ranging from 2 to 6 are obtained. The study is repeated to validate the numerical results of a model with control over different rib aspect ratios.

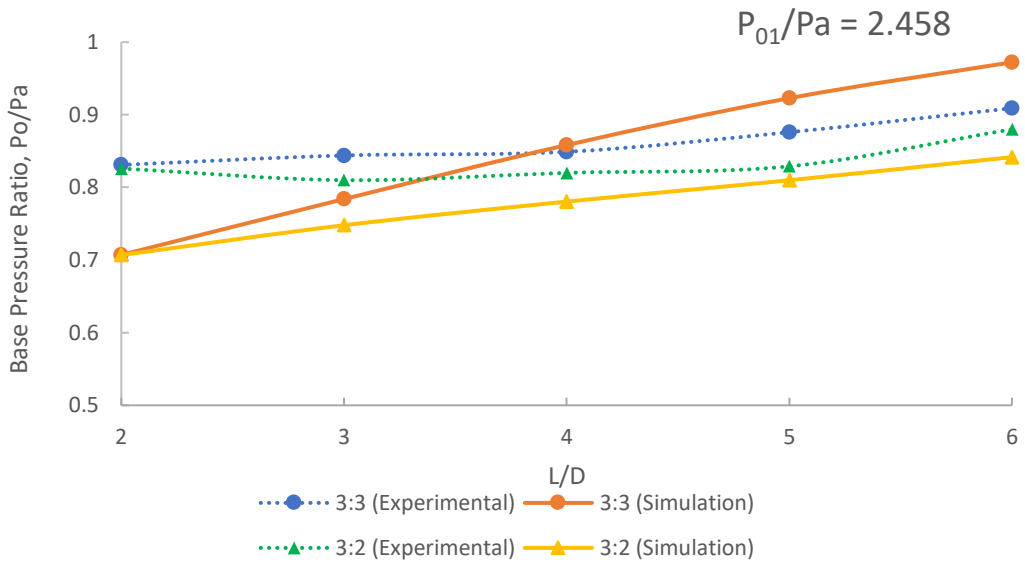

Fig. 4. Validation of previous work by Rathakrishnan [40]

Figure 4 demonstrates the current and earlier studies' base pressure ratio data curves [40]. The experimental values were denoted by dotted lines, while the simulation results obtained using ANSYS Fluent were represented by straight lines. The present numerical analysis exhibited a percentage discrepancy of less than 10% compared to the previous experimental study. Consequently, the current work met the criteria for acceptability. The curves exhibited a consistent pattern, with each point close to the subsequent one. As a result, based on the table and graph described before, the validation of the current work was successful.

3.7 Mesh Independence Study

Table 2 provides data from a mesh independence study, a crucial step in computational simulations to ensure that the results remain consistent regardless of the mesh refinement level. The element sizes range from the coarsest to the finest, with corresponding node and element counts for each mesh configuration. As the mesh becomes finer, the number of nodes and elements increases significantly, from 1,284 nodes and 1,145 elements in the coarsest mesh to 1,354,262 nodes and 1,351,303 elements in the finest mesh.

This study aims to determine the optimal mesh size for accurate simulations without unnecessary computational expense. The Table 2 shows a notable increase in nodes and elements as the mesh is refined. The coarsest mesh has relatively few nodes and elements, which means lower computational cost but potentially less accuracy. Conversely, the finest mesh offers the highest resolution at the expense of significant computational resources. The medium and fine meshes provide intermediate levels of refinement, offering a balance between accuracy and efficiency.

Based on the node and element numbers trends, the finest mesh will likely produce the most accurate results (Figure 5). However, continuing to refine the mesh beyond a certain point may offer diminishing returns in terms of accuracy while significantly increasing computational time. A critical assessment of this table would suggest that the "Fine" or "Finer" mesh configurations may represent the best balance between accuracy and computational efficiency. These configurations substantially increase nodes and elements compared to the medium meshes without reaching the computational expense of the finest mesh. If simulation results do not significantly change between the fine and finest meshes, further refinement to the finest mesh is unnecessary, as it would only increase

computational time without added benefit. Thus, the fine or finer mesh sizes are likely the best choices for further simulation.

Table 2
Mesh independence study

Element size	Coarsest	Coarse	Medium 1	Medium 2	Fine	Finer	Finest
Nodes	2997	3534	9582	17216	101106	293204	1482632
Elements	2808	3320	9720	16818	100248	291720	1479348

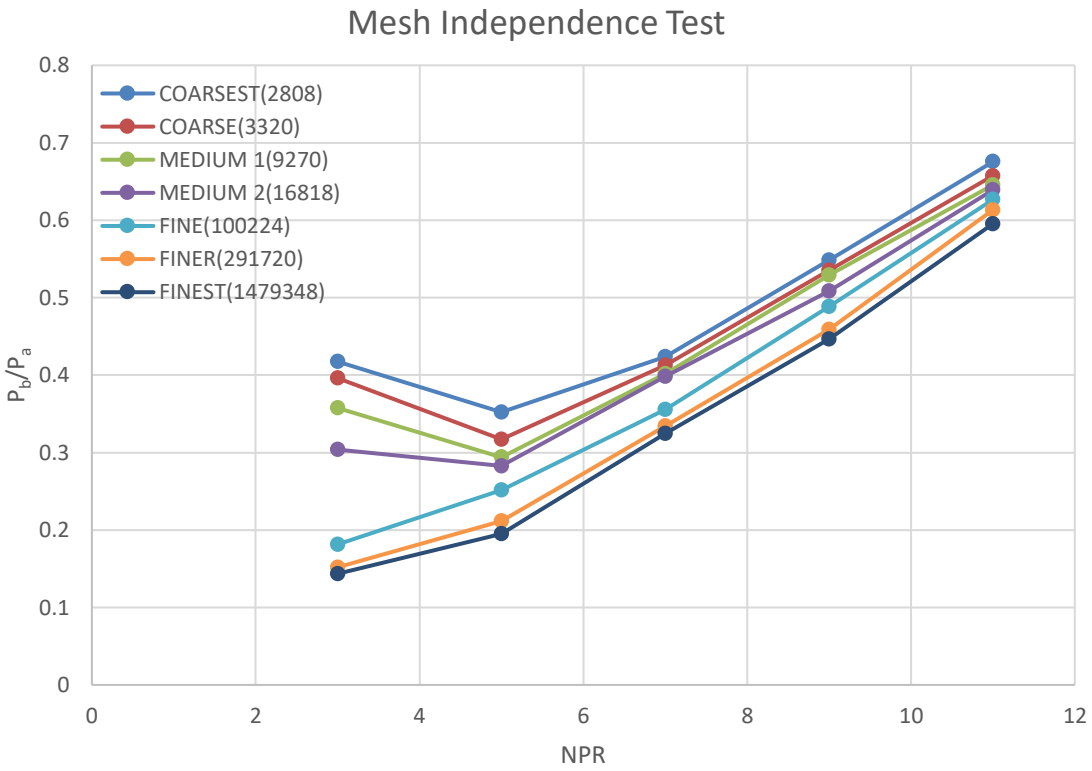

Fig. 5. Results of mesh check

4. Results and Discussions

Understanding the mechanics underlying the abruptly increased flow field would be instructive before interpreting the data. The nozzle exit boundary layer would grow as a free shear layer flows and meets the enlarged duct wall downstream. The reattachment point is the position of the flow attachment. The reattachment length is the distance from the base to the end of the reattachment. One or more vortices will be positioned between the reattachment point, the base, and the free shear layer edge; the primary vortex is the initial, more powerful one closest to the base, which pumps fluid from the base to the main flow on the other side of the free shear layer edge. At the base, low pressure is the result of this pumping motion. However, the pumping also becomes periodic because vortex shedding is periodic. As a result, there are variations in the base pressure. The base pressure fluctuations, however, were frequently found to be tiny and could be expressed as a mean value. The vortex motion's periodicity causes the duct's whole flow field to oscillate. The oscillations can become severe for certain combinations of geometrical factors and flow.

The flow Mach number and the reattachment control the primary vortex strength, which also significantly impacts the amount of suction at the base and the flow oscillations in the duct. Depending on whether the flow is over-expanded or under-expanded, an oblique shock ring or an

expansion fan ring is located at the nozzle outlet for supersonic Mach values. The flow accelerates and veers off when there is an expansion. Early reattachment and shorter reattachment length will result from this extra turning and the turning brought on by free expansion. When there is an oblique shock, the flow will be directed toward the duct centerline, delaying and lengthening the reattachment process. Therefore, the waves will significantly impact strength in any scenario since the base pressure and flow field oscillations depend on the primary vortex. The flow will encounter more vortices shed at the cavity if the duct has annular grooves. The base pressure may rise due to these smaller vortices acting as mixing promoters.

Figure 6 shows a view of the converging-diverging nozzle with duct and quarter-circle rib for orientation one. The Figure 6 shows that the curved part faces the flow from the nozzle first, whereas the straight part of the rib is demonstrated towards the trailing edge.

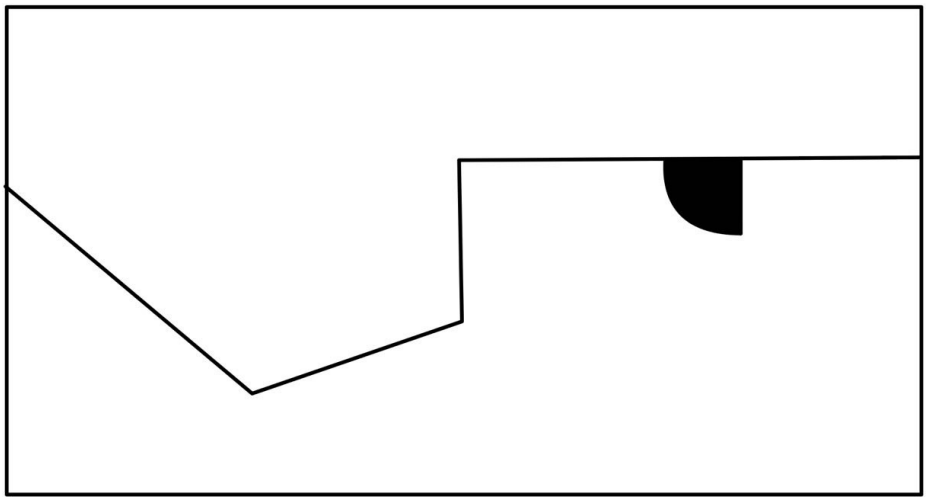

Fig. 6. A view of the nozzle and duct with rib

4.1 Base Pressure Results when the Rib is Located at 0.5D

The data extracted from the fluent software is gauge pressure. We add atmospheric pressure to convert it to absolute pressure, and then the base pressure is made non-dimensional by dividing it by atmospheric pressure. This study was conducted at Mach M = 2.0 for a duct diameter of 22 mm, for different rib radii ranging from 1 mm to 4 mm, and for duct lengths from L = 1D to 6D. The NPRs of the present study range from 3 to 11. The NPR needed for correct expansion is 7.83, and the expansion levels for NPRs studied are 0.38, 0.64, 0,894, 1.15, and 1.41. As the jet exits the nozzle, it experiences over-, correct, and under-expansion due to the NPR range used in this test. It is commonly recognized that an oblique shock or expansion fan will be placed at the nozzle lip for over and under-expanded situations. The base pressure variation as a function of Mach number, L/D, and NPR is shown to grasp how the degree of expansion affects the base pressure both with and without control. Base pressure for both overexpanded and underexpanded jets is included in the NPR 3 data along with L/D. The shear layer emerging from the nozzle will be bent towards the nozzle center line by the shock if there is an oblique shock at the nozzle exit. As opposed to a situation without a shock, this will cause the reattachment to take longer to occur. As is often known, the base pressure is affected by changes in the reattachment length, which also significantly impacts the base vortex.

In the same way, an expansion fan reduces the reattachment length compared to a case without one by deflecting the shear layer exiting the nozzle closer toward the base. Both over- and under-expansion operations are crucial to base pressure analysis because they create an oblique shock or expansion fan at the nozzle outlet. The findings indicate that factors other than over- and under-

expansion affect the base pressure level. However, determining the base pressure level depends on the degree of under- or overexpansion.

Figure 7(a)-(f) show the findings of this study when the quarter-circle rib is placed at 11 mm from the base, with different rib radii ranging from 1 mm to 4 mm, for various duct lengths ranging from L = 22 mm to L = 132 mm at different level of expansion. For the most petite duct lengths of 22 mm, the outcomes of this study are shown in Figure 7(a). The base pressure results for this duct length differ from the other lengths. The reason for this trend is that the duct length is the smallest and is insufficient for the flow to get attached to the duct wall, and more so, there will be a strong influence on the ambient pressure, which will try to impact the flow field inside the duct. There is a decreasing trend in the base pressure without control; rib radii are 1 mm and 2 mm. However, when NPR is seven and above, there is an increasing trend in the base pressure except for rib radii 3 mm and 4 mm, as these ribs are in a position to generate powerful vortices and push additional mass towards the base area, resulting in higher values of the base pressure. The base pressure ratio values at NPR 11 are 0.4, 0.75, 1.05, 1.4, and 1.78, respectively. When we look at the base pressure data for other duct lengths, their magnitude is nearly the same except for minor fluctuations, and these variations are expected due to the variations in the duct size. Because of the changes in the duct size, the influence of the ambient pressure will also vary, resulting in fluctuations in their values.

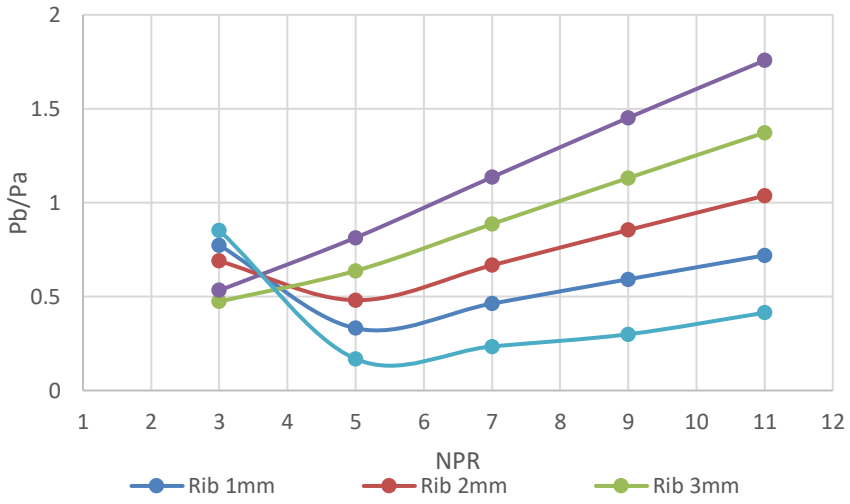

(a) L/D = 1

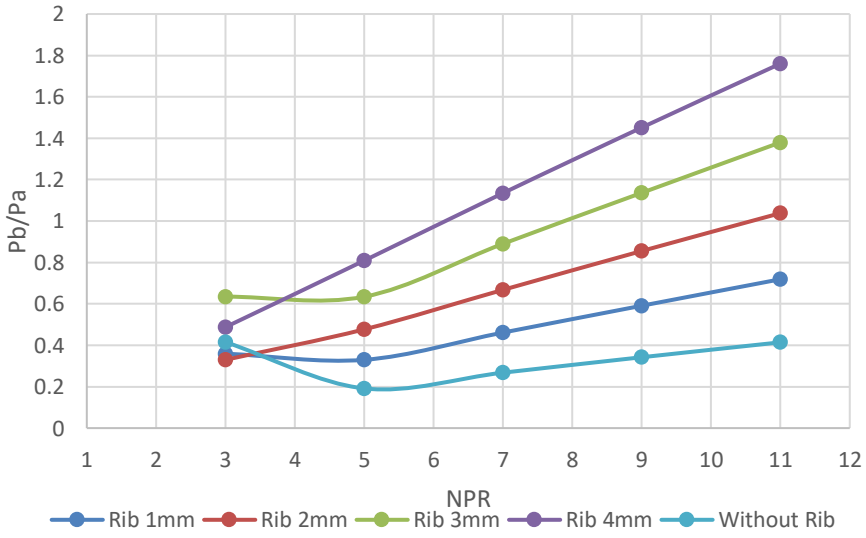

(b) L/D = 2

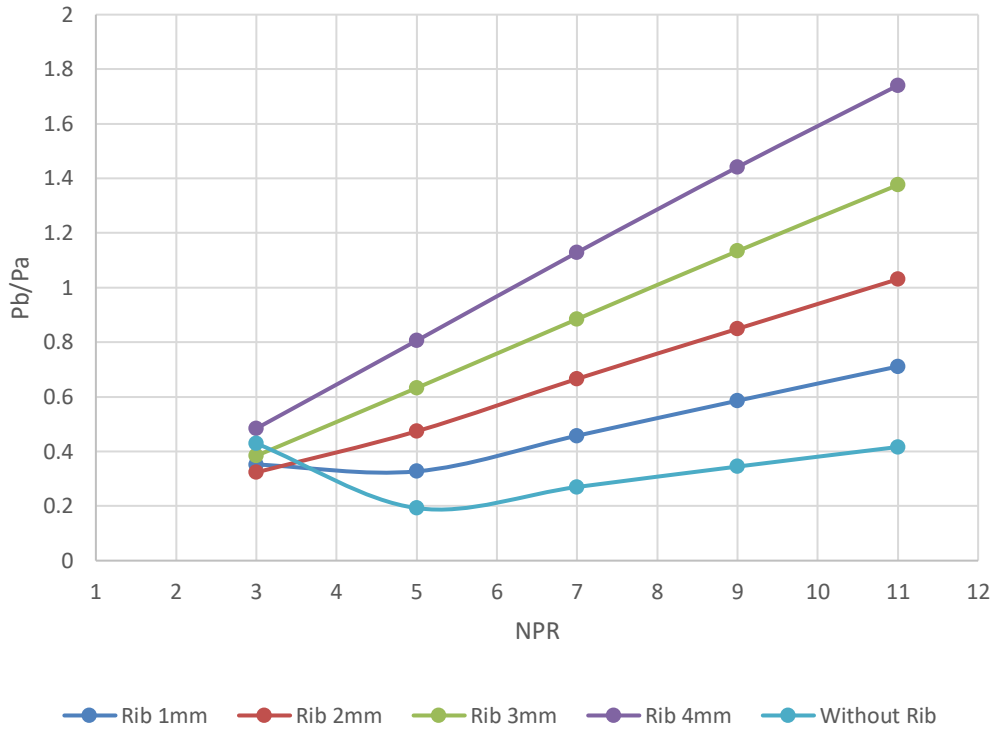
Pb/Pa
NPR
Rib 1mm
Rib 2mm
Rib 3mm
Rib 4mm
Without Rib

(c) L/D = 3

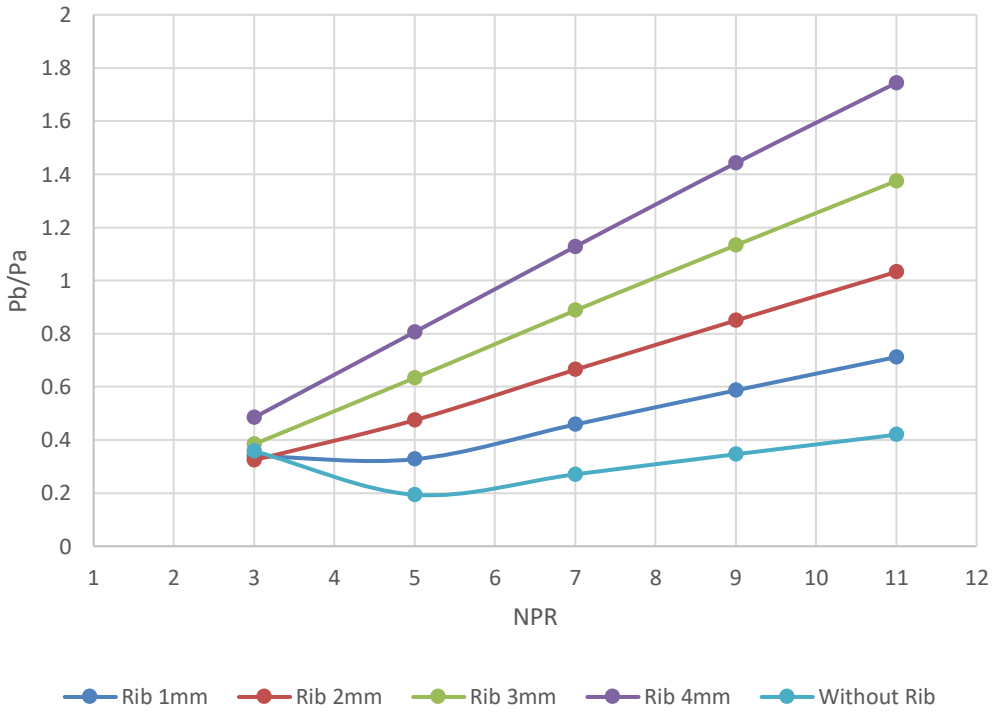
Pb/Pa
NPR
Rib 1mm
Rib 2mm
Rib 3mm
Rib 4mm
Without Rib

(d) L/D = 4

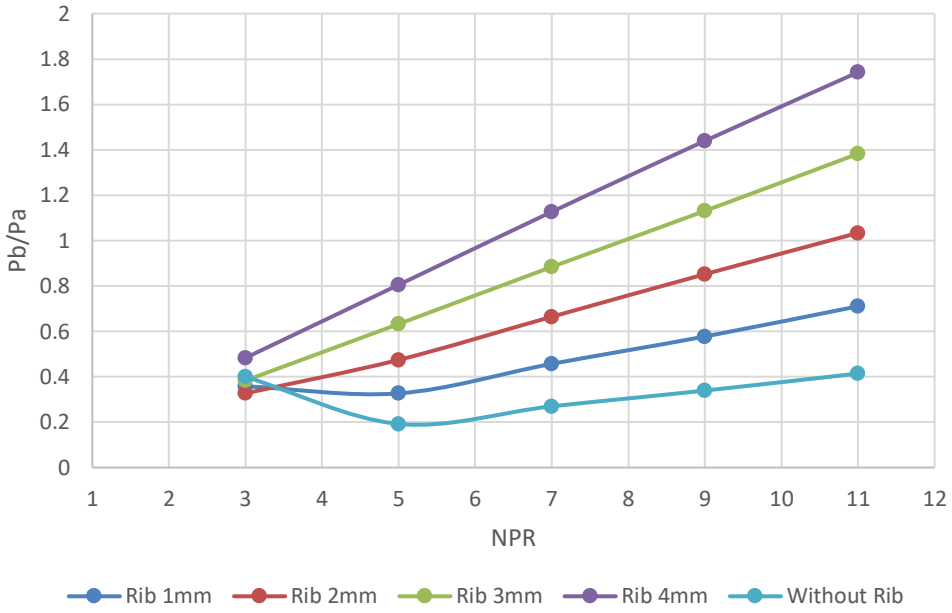

(e) L/D = 5

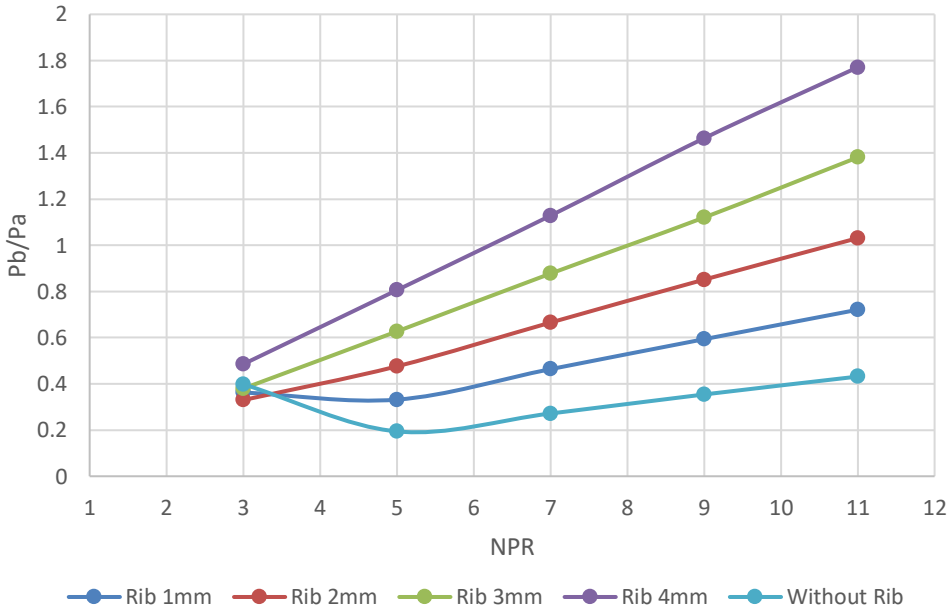

(f) L/D = 6

Fig. 7. Base pressure Vs. NPR for various duct lengths

4.2 Base Pressure Results when the Rib is Located at 1D

Figure 8(a)-(e) display the findings of the study for ribs placement at 22 mm, for duct lengths L = 1D to 6D, for all the four rib radii ranging from 1 mm to 4 mm, and NPRs ranging from 3 to 11. Base pressure results for this rib location are different from the previous case. The base pressure values for the without control case and 1 mm rib case are identical, and passive control cannot impact the flow field except for NPR in the range of 3 to 5 when the nozzle is over-expanded, as seen in Figure 8(a).

Furthermore, the base pressure ratio for this rib location is nearly the same as for the 11 mm rib placement. These behaviors are attributed to the formation of oblique shock waves, Mach waves, and oblique shock waves. The base pressure ratio for rib radii 2 mm, 3 mm, and 4 mm are 0.75, 1.25,

and 1.78. This study gives users vast options for selecting rib location, rib radius, duct length, and NPR.

Similar results are seen for the remaining duct lengths; the base pressure ratio remained nearly the same as was observed for duct lengths L = 2D. The base pressure also remains almost the same, except for a minor change for higher duct lengths, as the influence of the ambient pressure will be the least for more considerable duct lengths, as seen in Figure 8(b) to Figure 8(e).

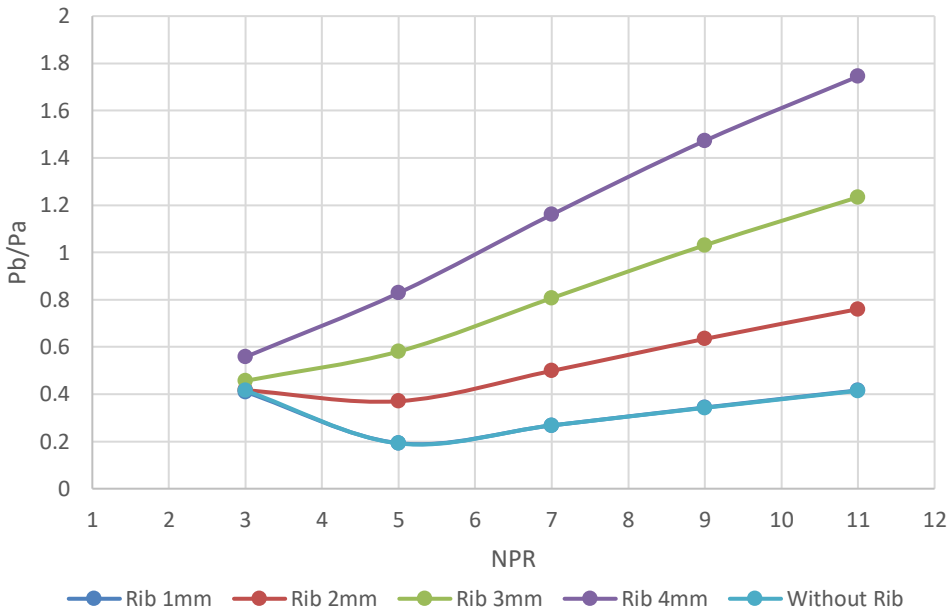

(a) L/D = 2

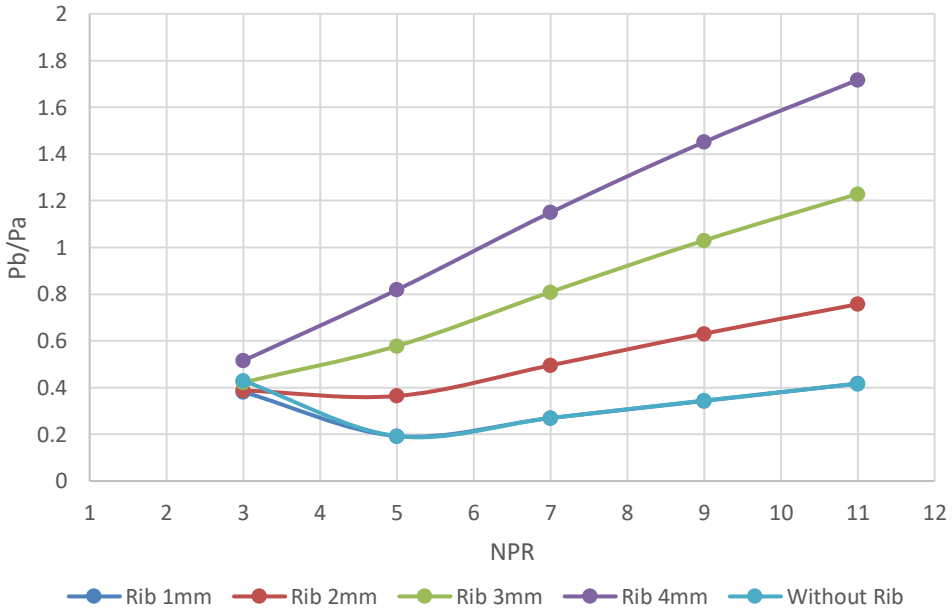

(b) L/D = 3

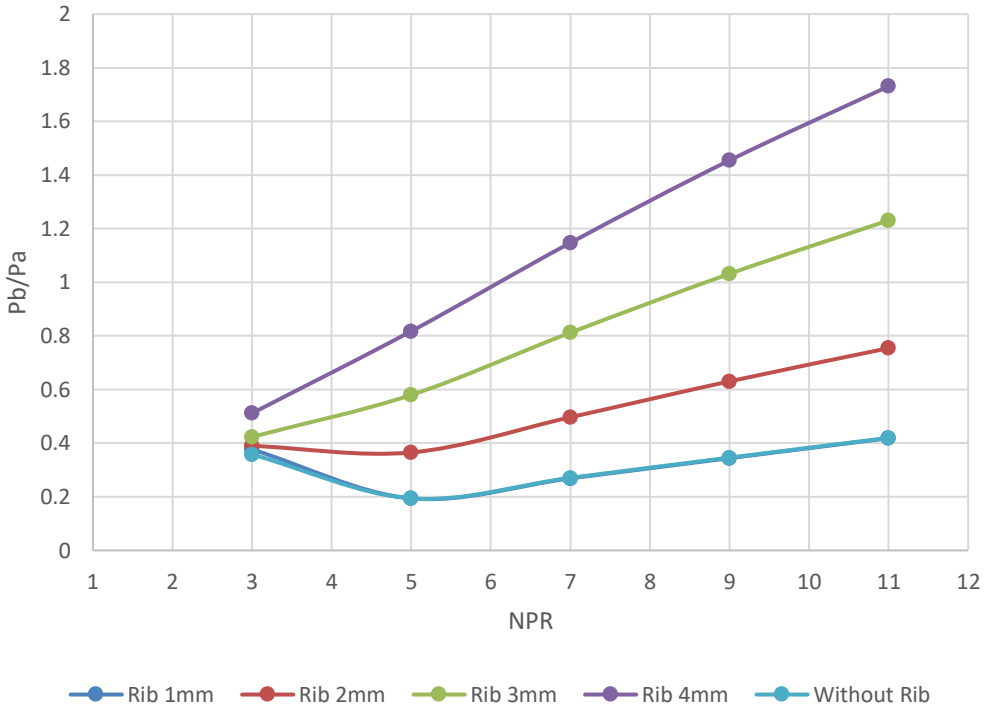
Pb/Pa
NPR
Rib 1mm
Rib 2mm
Rib 3mm
Rib 4mm
Without Rib

(c) L/D = 4

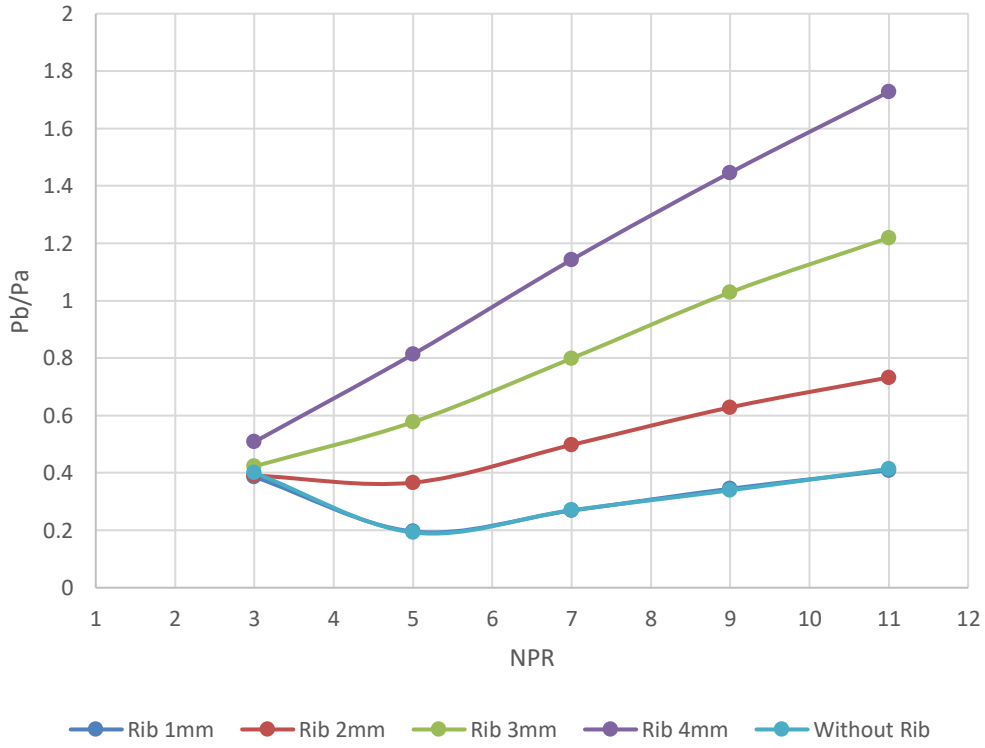
Pb/Pa
NPR
Rib 1mm
Rib 2mm
Rib 3mm
Rib 4mm
Without Rib

(d) L/D = 5

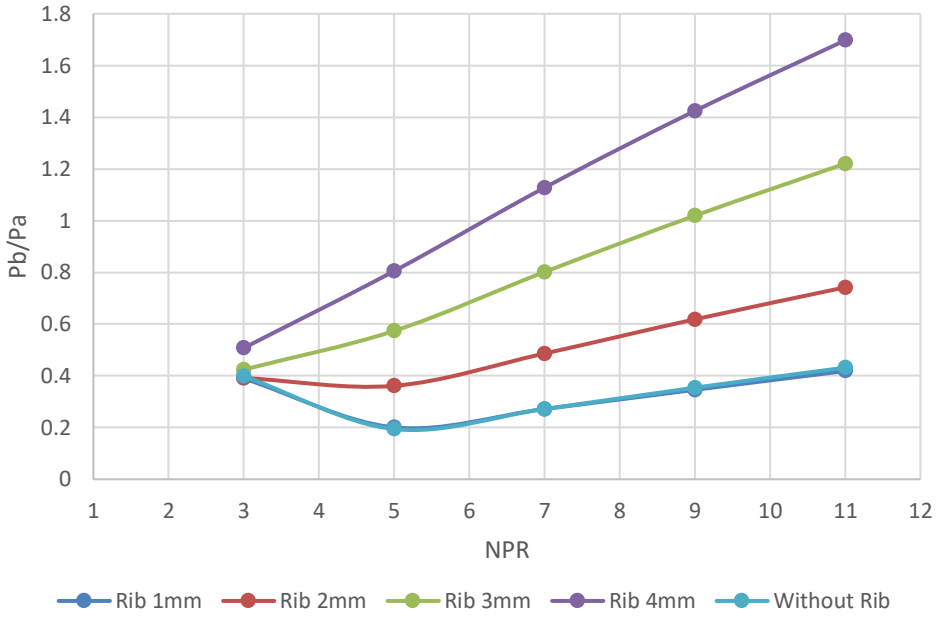

(e) L/D = 6

Fig. 8. Base pressure Vs. NPR for various duct lengths

4.3 Base Pressure Results when the Rib is Located at 1.5D

When the passive control in the form of ribs is located 33 mm from the base, the study's findings are shown in Figure 9(a)-(e) for the same range of rib radius, duct lengths, and level of expansion ranging from 3 to 11. As seen earlier, without control, when a rib of 1 mm radius is placed within the same range of NPRs, similar trends are observed. The base pressure ratio for rib radii 2 mm, 3 mm, and 4 mm are 0.9, 1.55, and 2.3. Results show a linear increase in the base pressure magnitude with shifting rib locations towards the downstream, except for marginal variations in the base pressure values. However, the magnitude is nearly the same. These variations are attributed to the impact of the ambient pressure on the flow field inside the duct.

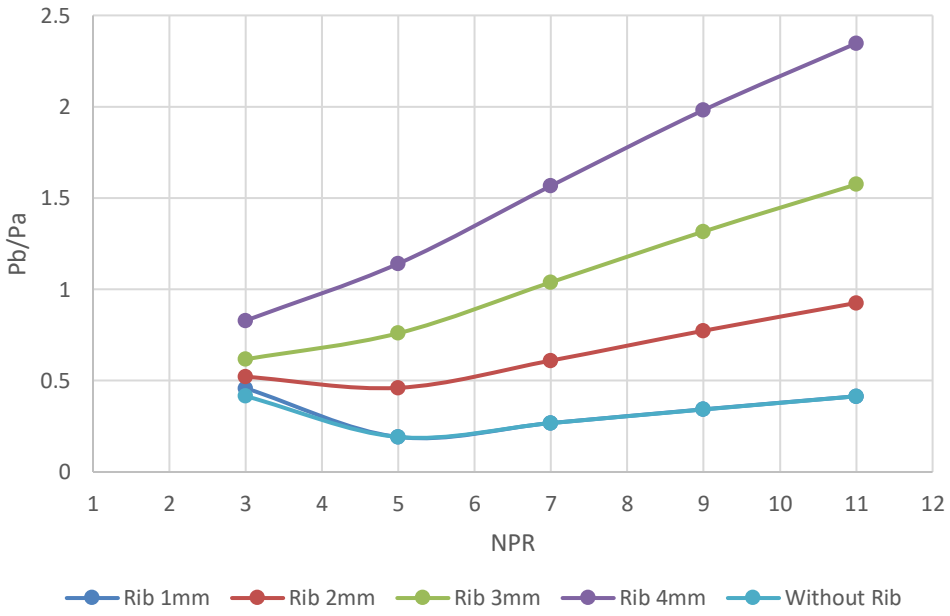

(a) L/D = 2

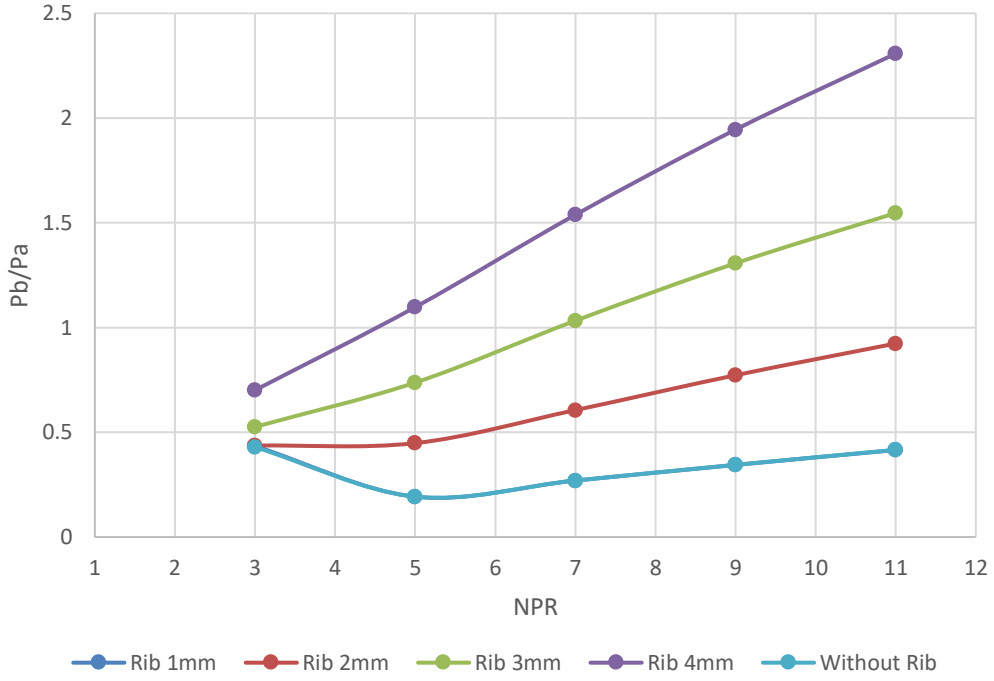
2.5
2
1.5
1
0.5
0
Pb/Pa
1
2
3
4
5
6
7
8
9
10
11
12
NPR
Rib 1mm
Rib 2mm
Rib 3mm
Rib 4mm
Without Rib

(b) L/D = 3

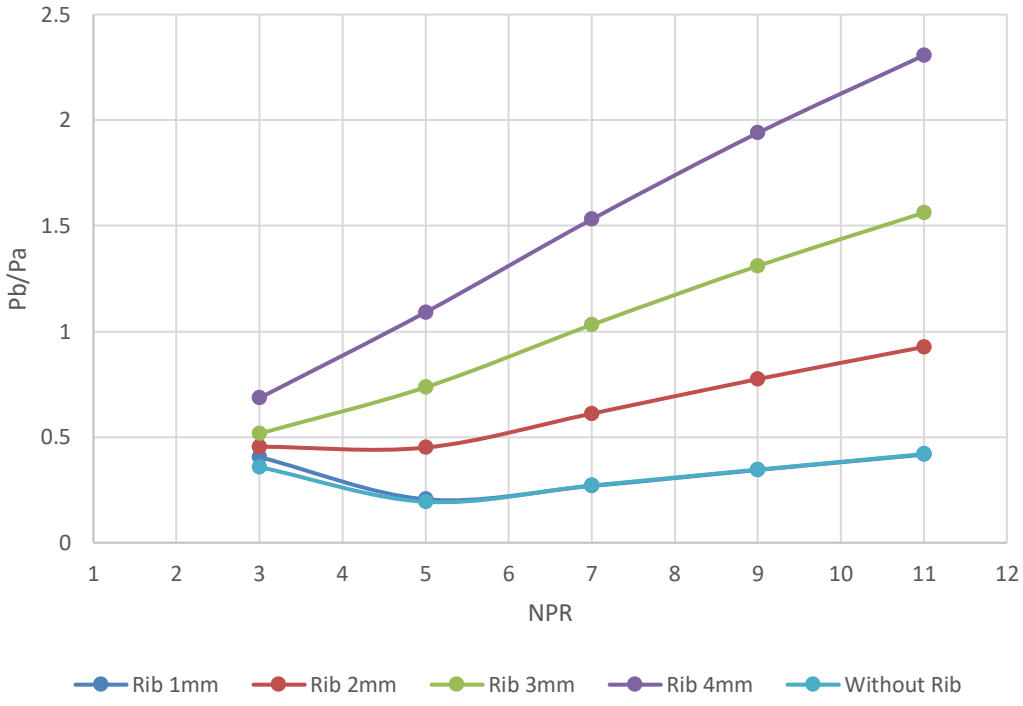
2.5
2
1.5
1
0.5
0
Pb/Pa
1
2
3
4
5
6
7
8
9
10
11
12
NPR
Rib 1mm
Rib 2mm
Rib 3mm
Rib 4mm
Without Rib

(c) L/D = 4

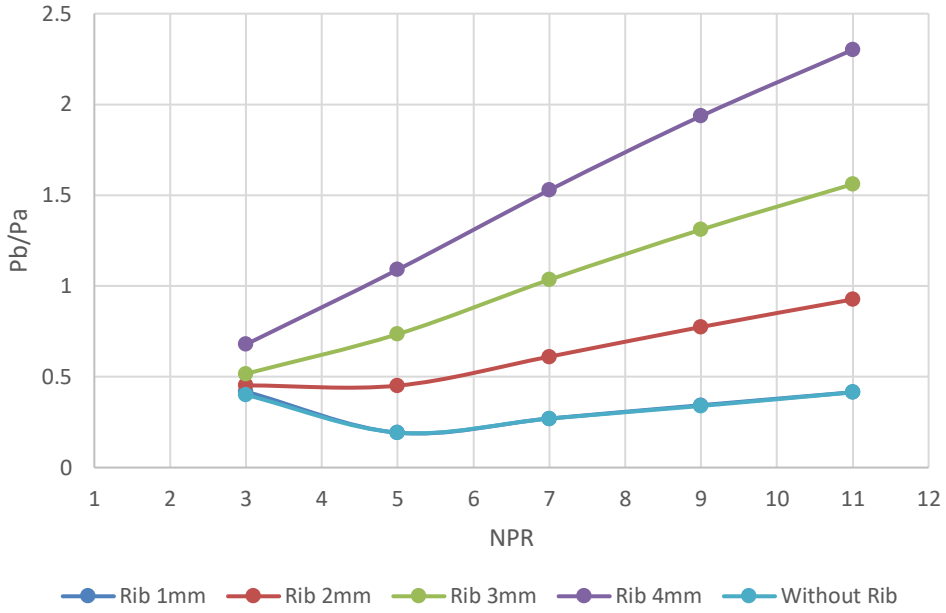

(d) L/D = 5

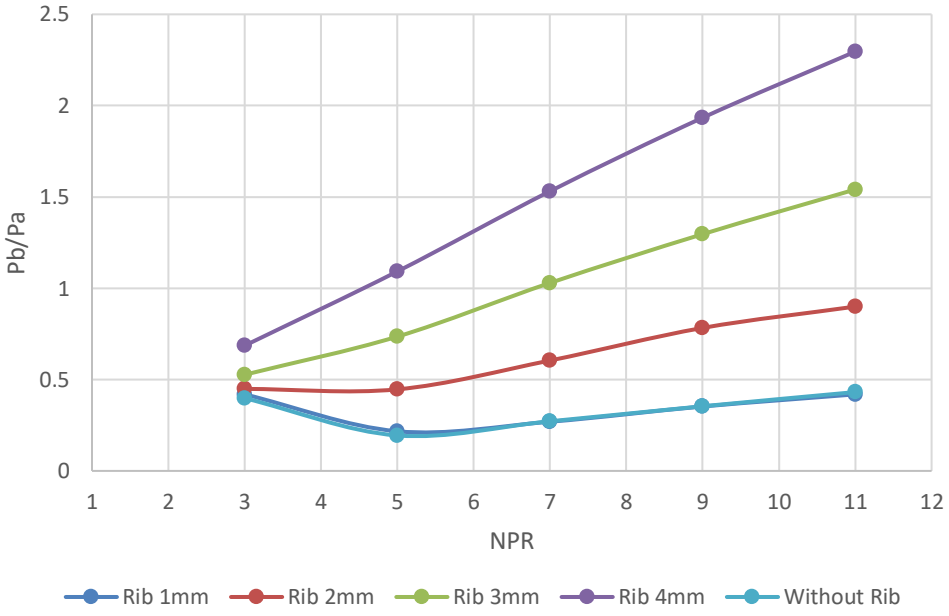

(e) L/D = 6

Fig. 9. Base pressure Vs. NPR for various duct lengths

4.4 Base Pressure Results when the Rib is Located at 2D

Figure 10(a)-(d) shows the results of this study for rib radii 1 mm, 2 mm, 3 mm, and 4 mm for duct lengths ranging from L = 1D to 6D for NPRs in the range from 3 to 11. From these results, it is seen that there is a considerable increase in the base pressure for all the rib radii at different duct lengths. As discussed earlier, the rib with a 1 mm radius and without control show similar results. That means that a 1 mm radius cannot influence the flow field. For maximum rib radius, the base pressure attained is 2.8, followed by 2.3 and 1 when the rib radius is 3 mm and 2 mm. Figure 10(b) to Figure 10(d) represent similar results as seen for duct length of 66 mm in Figure 10(a). However, there is marginal variation in the base pressure due to an increase in the duct lengths for lower duct lengths,

and there will be the influence of the atmospheric pressure; however, the impact of the ambient pressure will diminish with an increase in the duct length.

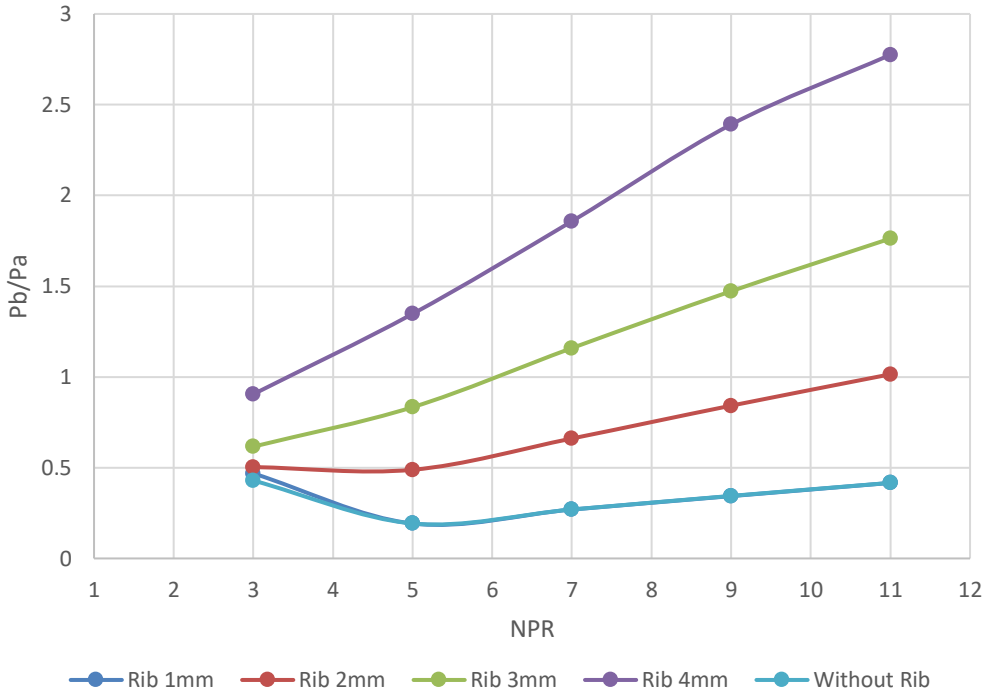

(a) L/D = 3

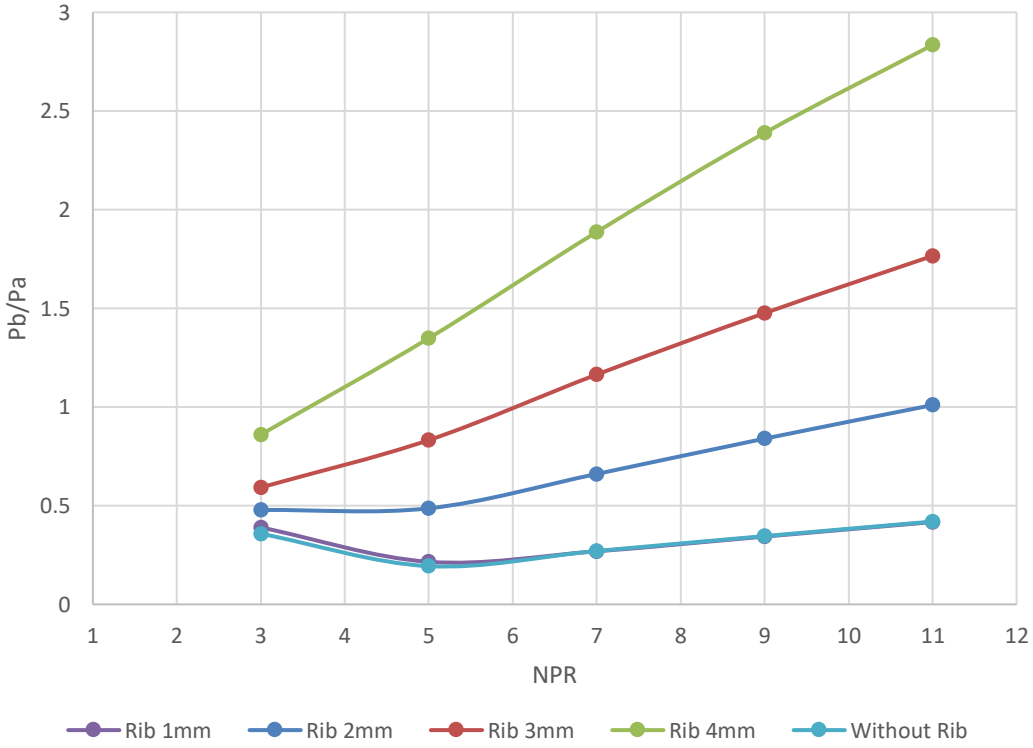

(b) L/D = 4

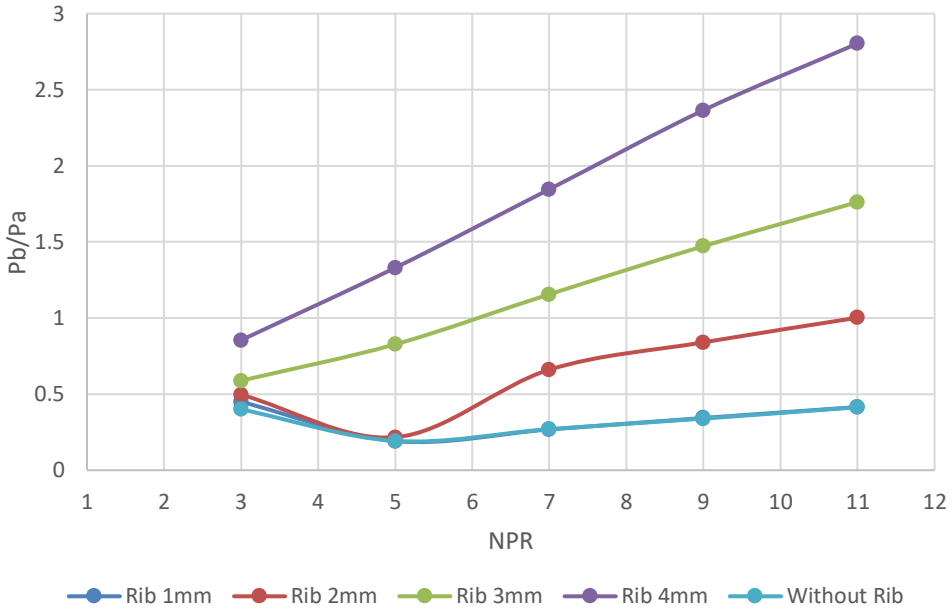

(c) L/D = 5

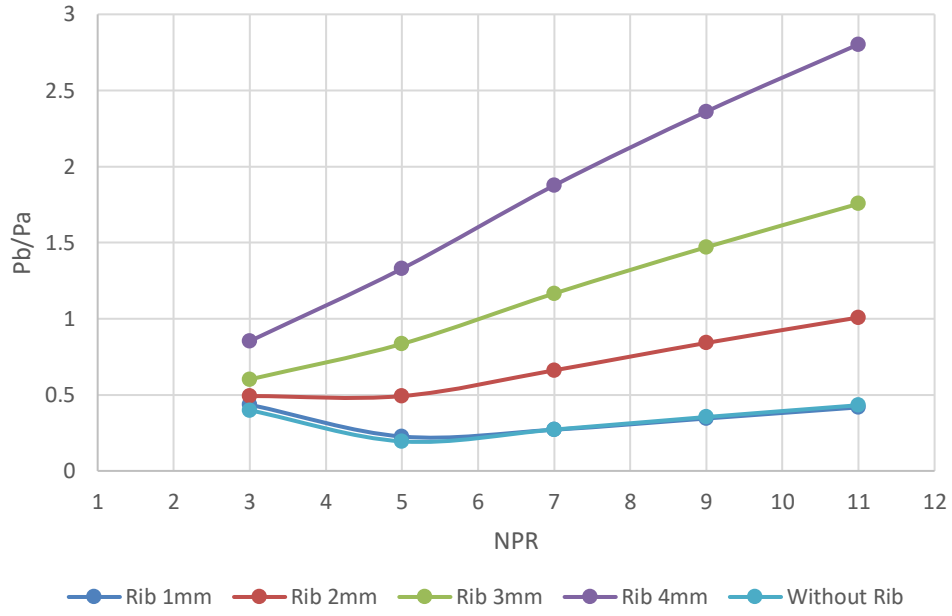

(d) L/D = 6

Fig. 10. Base pressure Vs. NPR for various duct lengths

4.5 Base Pressure Results When the Rib is Located at 3D

For the farthest location of the rib at 3D (i.e., 66 mm from the base), the base pressure results for four rib radii ranging from 1 mm to 4 mm, duct length ranging from L = 88 mm to 132 mm for various NPRs ranging from 3 to 11 are shown in Figure 11(a)-(c). Figure 11(a) shows that due to the further shift in the rib location towards the downstream, there is a further rise in the base pressure. The base pressure results without a rib, and the base pressure magnitude for a 1 mm rib radius is the same as that observed for other rib locations. Hence, this phenomenon is independent of the rib placement but firmly dependent on the rib radius. When we look at the findings of this study, other duct lengths, namely L/D = 110 mm and 132 mm, the base pressure ratio nearly remains identical. The values of the base pressure ratios are 0.48. 1.08, 2.0, and 2.8. However, in most cases, it will remain the same.

However, there are minor differences due to the different duct lengths. Therefore, depending upon the mission requirement, one can take a final call for the rib location, rib radius, L/D ratio, and level of expansion to accomplish the user's requirements.

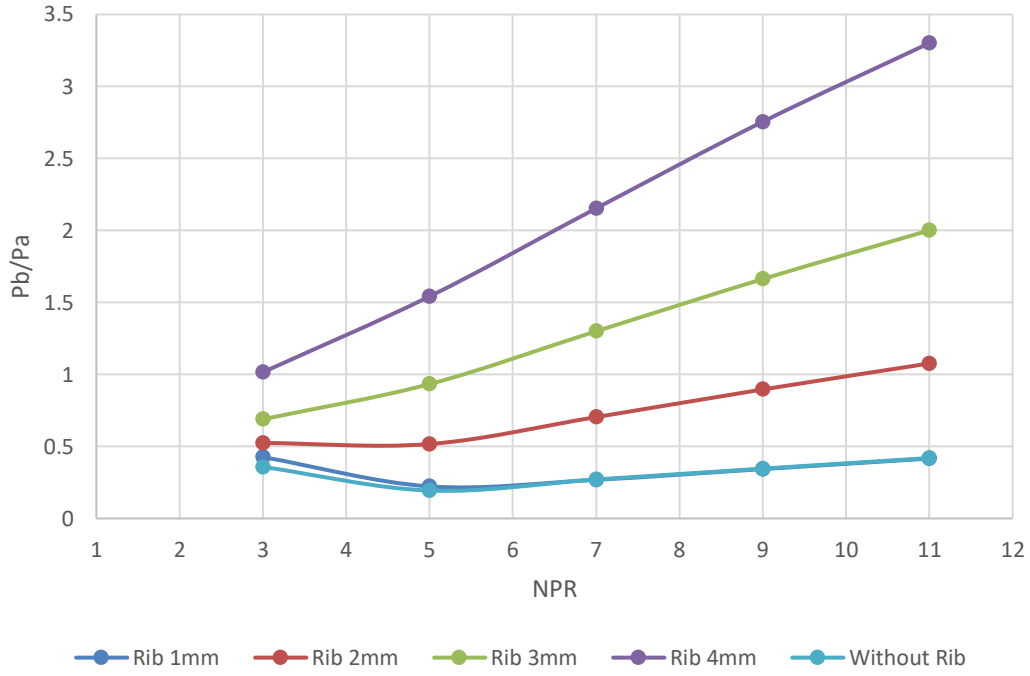

(a) L/D = 4

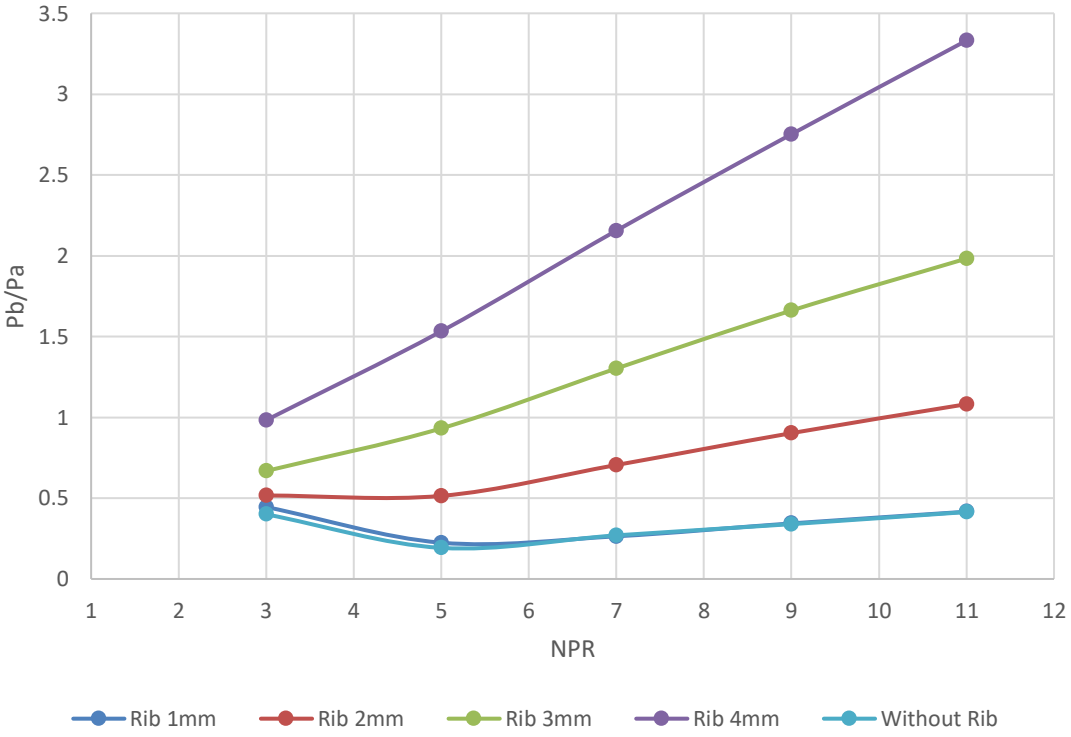

(b) L/D = 5

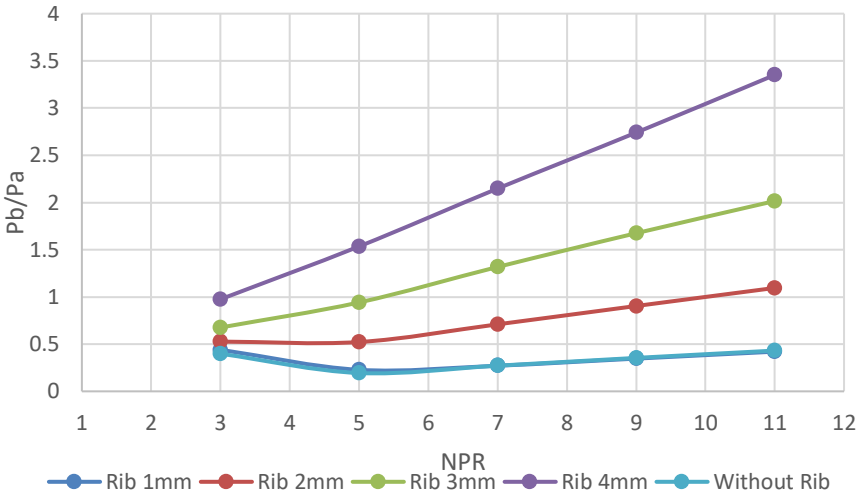

(c) L/D = 6

Fig. 11. Base pressure Vs. NPR for various duct lengths

4.6 Pressure Contours

The pressure contours delineate the flow characteristics associated with a rib diameter measuring 4 mm and a duct length-to-diameter (L/D) ratio of 5, as shown in Figure 12(a)-(c). The rib is positioned at a distance of 1D from the nozzle exit. These figures show various scenarios for three distinct NPR values. NPR = 3: Initial expansion level, NPR = 7: Intermediate expansion, and NPR = 11: Maximum expansion level studied.

When NPR = 3, the base pressure remains comparatively low, characterized by a distinct suction region at the base of the recirculation zone. However, the dynamics of fluid behavior can be complex because various factors influence the effectiveness of the rib design.

When NPR = 7, the suction zone commences diminishing while base pressure begins to escalate. However, the dynamics at play could vary under different circumstances because the interaction between pressure gradients and structural features is complex.

When NPR = 11, the suction zone experiences a substantial reduction; moreover, the base pressure attains its peak for this configuration. That indicates that the maximum base pressure, corresponding to a rib diameter of 4 mm, is realized at high NPRs. This observation is in alignment with the contour trends noted herein.

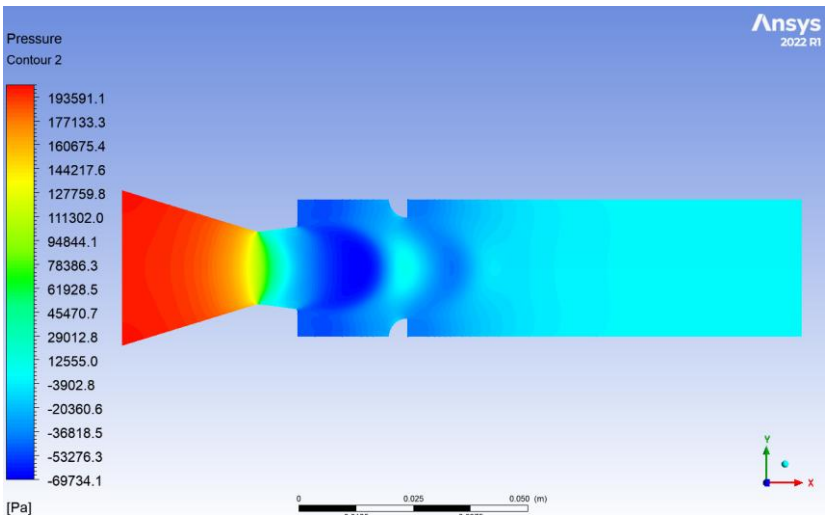

(a) NPR = 3

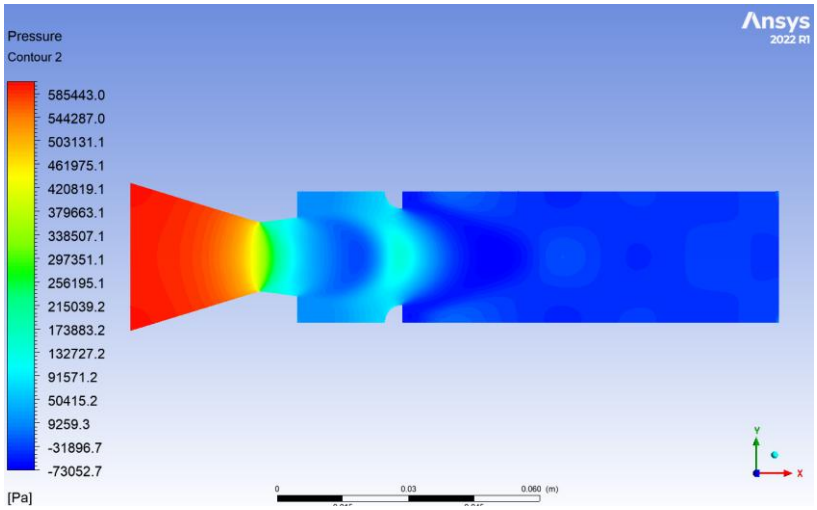

(b) NPR = 7

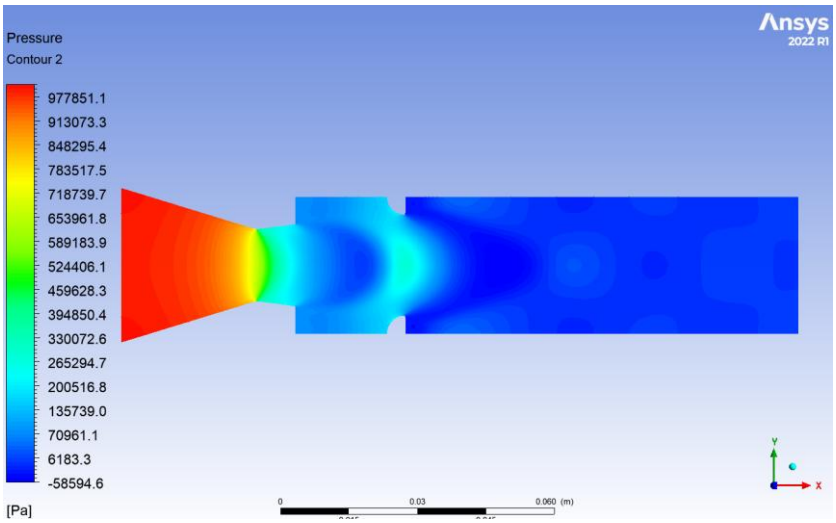

(c) NPR = 11

Fig. 12. Pressure contours for rib diameter 4 mm, L/D=5 and rib location at 1D

4.7 Velocity Contours

The velocity contours are delineated for a rib diameter of 4 mm, a duct length-to-diameter (L/D) ratio of 5, and the rib strategically positioned at 1D from the nozzle exit are shown in Figure 13(a)-(c). The scenarios are assessed for three NPR values. NPR = 3: Low expansion level, NPR = 7: Intermediate expansion, and NPR = 11: High expansion level.

When NPR = 3, flow separation and recirculation predominate near the base at lower NPR, significantly reducing velocities within the downstream region.

When NPR = 7, as the NPR increases, the flow commences to stabilize, with higher velocity regions becoming evident near the duct walls. The recirculation zone, interestingly, diminishes in size. However, it is noteworthy that the relationship between rib radius and flow dynamics may not be straightforward because other factors could also influence these outcomes.

When NPR = 11, at elevated NPR, the flow manifests near-optimal reattachment, exhibiting minimal recirculation and elevated velocities throughout the duct.

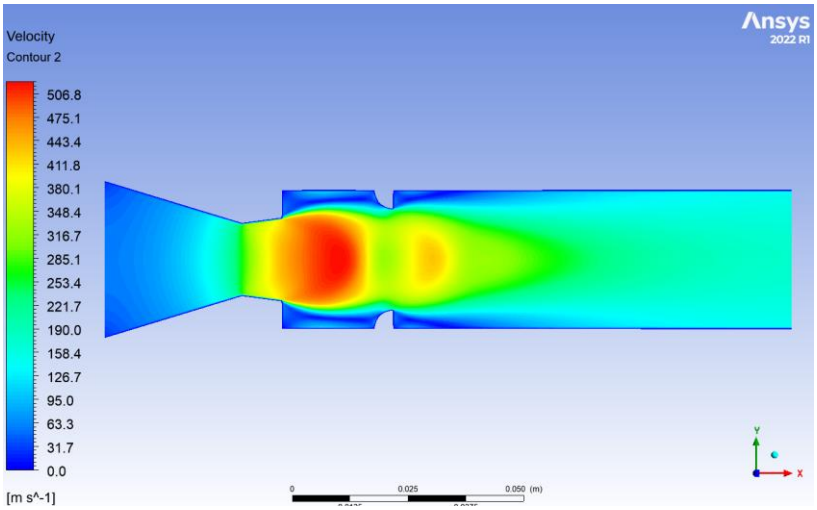

(a) NPR = 3

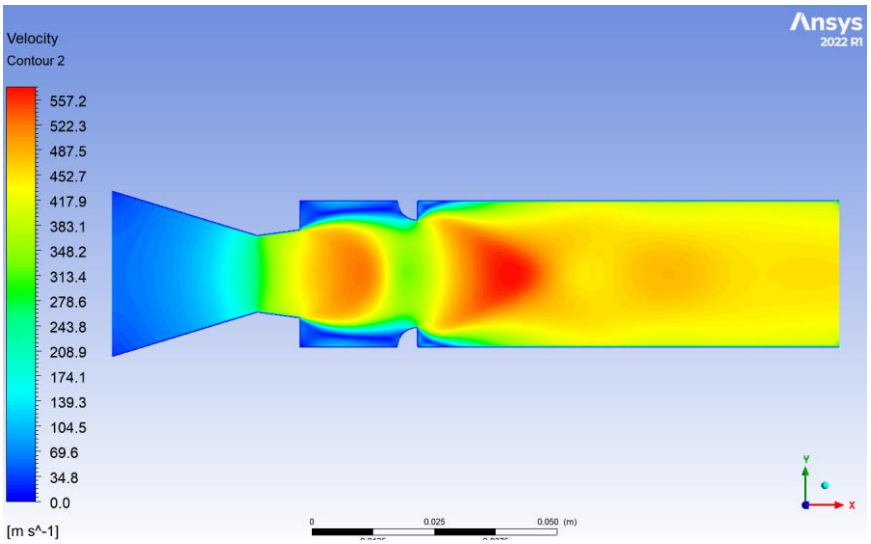

(b) NPR = 7

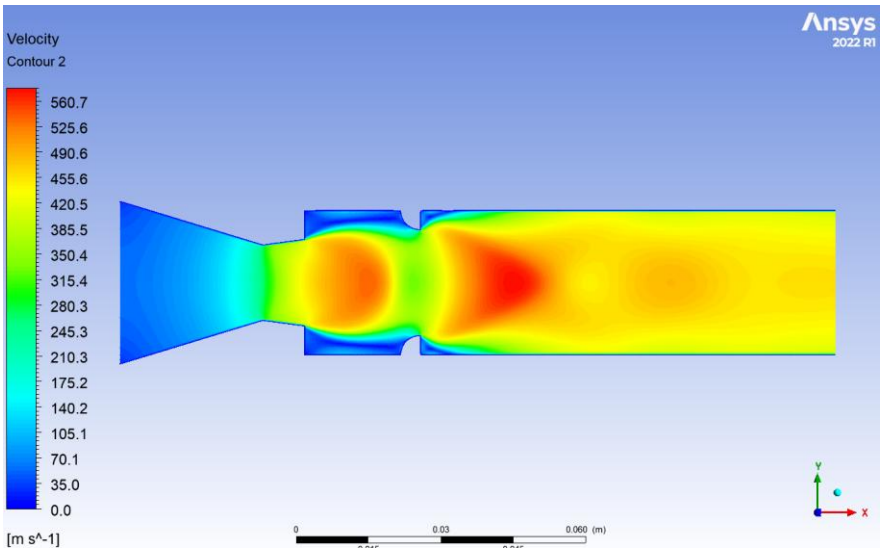

(c) NPR = 11

Fig. 13. Velocity contours for rib diameter 4 mm, L/D=5 and rib location at 1D

4.8 Velocity Streamlines

Figure 14(a)-(c) show the velocity streamlines associated with a rib diameter of 4 mm, a length-to-diameter (L/D) ratio of 5, and rib placement at 1D, all under conditions of varying nozzle pressure ratios (NPR). When NPR = 3, the flow is predominantly characterized by extensive recirculation zones and diminished velocities proximate to the base. This observation substantiates the assertion that the rib is less productive at lower NPR, primarily because of adverse pressure gradients. Conversely, at NPR = 7, there is a notable reduction in recirculation zones, coupled with an emergence of elevated velocities adjacent to the duct walls. Here, the rib begins to exert a significant influence on flow reattachment. At NPR = 11, the streamlines exhibit a near-complete reattachment with minimal recirculation. In this scenario, the rib realizes its peak effectiveness at elevated NPR.

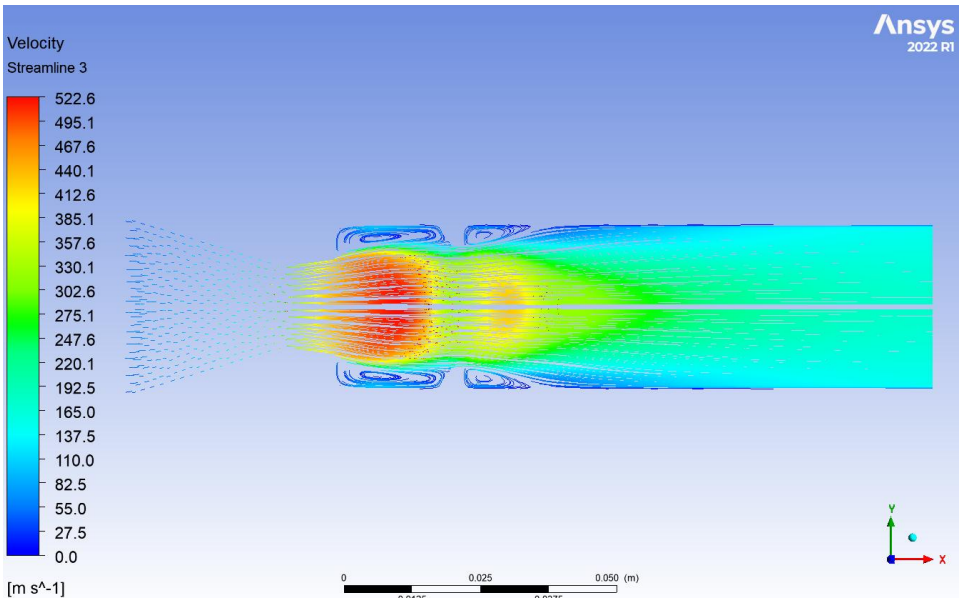

(a) NPR = 3

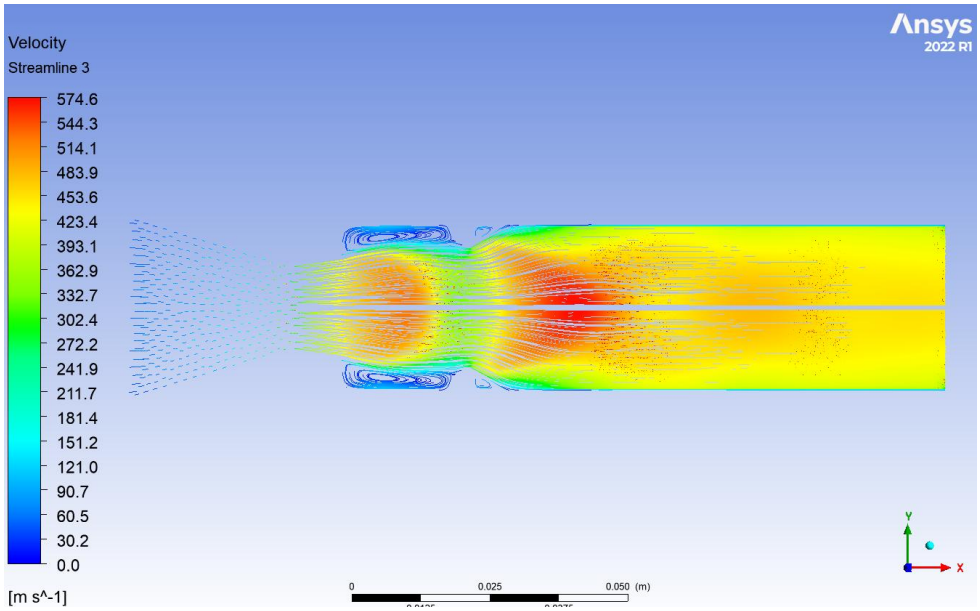

(b) NPR = 7

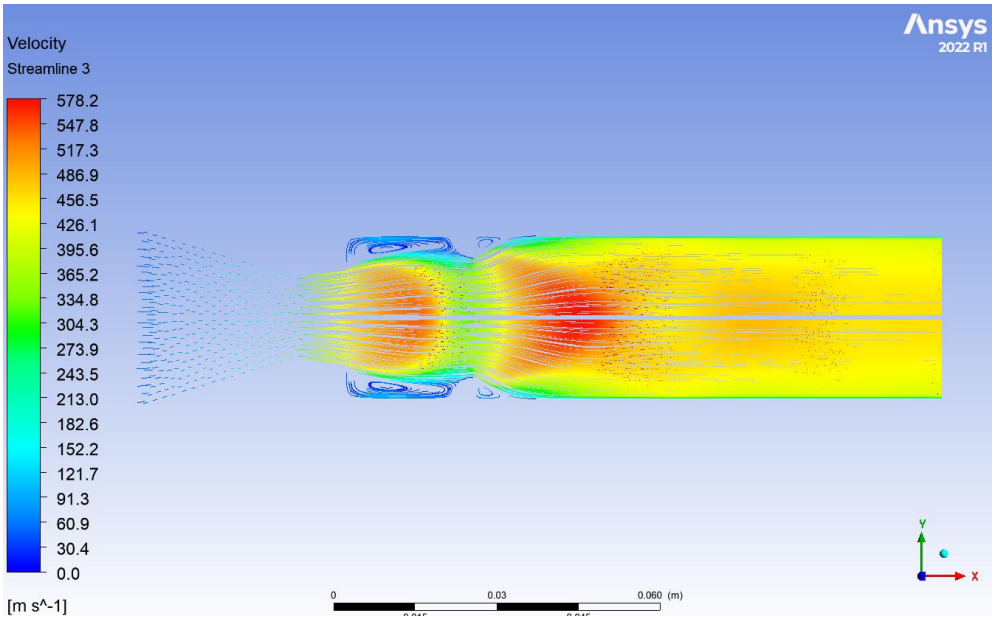

(c) NPR = 11

Fig. 14. Velocity streamlines for rib diameter 4 mm, L/D=5 and rib location at 1D

5. Conclusions

Based on the deliberations undertaken in the previous section, we may infer the following. When the rib is located at 11 mm inside the duct, there is a declining trend without control, and also when rib radii are 1 mm and 2 mm. However, this declining trend is reversed from NPR = 7 and above. Furthermore, it is seen that for rib radii in the range of 3 mm and 4 mm, there is a progressive increase in the base pressure right from NPR = 3. It continues to NPR = 11, and the base pressure ratio attained is 1.8 for a rib radius of 4 mm. Even though there is a change in the location of the rib, there is no augmentation in the base pressure values. When ribs are further downstream to 33 mm, the maximum base pressure ratio achieved is 2.3. It is also seen that for the remaining last two positions of the ribs downstream at 44 mm and 66 mm, the maximum base pressure ratios attained are 2.8 and 3.4. This study has provided a database that one can use to design and development of aerospace vehicles. These results are case-sensitive, and one must use them on a case-to-case basis. Base suction is reduced considerably for the highest rib radius of 4 mm. Therefore, a quarter circle rib with the highest rib radius of 4mm is recommended if the user's/mission requirement is needed to raise base pressure many folds. If the mission requires increasing the base pressure equal to ambient pressure or making base suction equal to zero, then a 2 mm rib radius is sufficient to achieve the mission requirement. Therefore, depending upon the mission requirement, one can take a final call for the rib location, rib radius, L/D ratio, and level of expansion to accomplish the user's requirements. These results are noteworthy, but the technology demonstration and authors have created a database that can be utilized by the defense forces in designing and developing missiles, unguided rockets, aircraft bombs, and artillery shells.

Acknowledgement

This research was not funded by any grant.

References

[1] Wick, Robert S. "The effect of boundary layer on sonic flow through an abrupt cross-sectional area change." *Journal of the Aeronautical Sciences* 20, no. 10 (1953): 675-682. https://doi.org/10.2514/8.2794

[2] Pathan, Khizar Ahmed, Prakash S. Dabeer, and Sher Afghan Khan. "Effect of nozzle pressure ratio and control jet location to control base pressure in suddenly expanded flows." *Journal of Applied Fluid Mechanics* 12, no. 4 (2019): 1127-1135. https://doi.org/10.29252/jafm.12.04.29495

[3] Pathan, Khizar Ahmed, Syed Ashfaq, Prakash S. Dabeer, and Sher Afgan Khan. "Analysis of Parameters Affecting Thrust and Base Pressure in Suddenly Expanded Flow from Nozzle." *Journal of Advanced Research in Fluid Mechanics and Thermal Sciences* 64, no. 1 (2019): 1-18.

[4] Fiqri, Muhammad Ikhwan, Khizar Ahmed Pathan, and Sher Afghan Khan. "Control of Suddenly Expanded Flow with Cavity at Sonic Mach Number." In *International Conference on Advances in Heat Transfer and Fluid Dynamics*, pp. 3-15. Singapore: Springer Nature Singapore, 2022. https://doi.org/10.1007/978-981-99-7213-5_1

[5] Aqilah, Nur, Khizar Ahmed Pathan, and Sher Afghan Khan. "Passive Control of Base Flow at Supersonic Mach Number for Area Ratio 4." In *International Conference on Advances in Heat Transfer and Fluid Dynamics*, pp. 37-50. Singapore: Springer Nature Singapore, 2022. https://doi.org/10.1007/978-981-99-7213-5_4

[6] Pathan, Khizar A., Prakash S. Dabeer, and Sher A. Khan. "Enlarge duct length optimization for suddenly expanded flows." *Advances in Aircraft and Spacecraft Science* 7, no. 3 (2020): 203-214. https://doi.org/10.12989/aas.2020.7.3.203

[7] Pathan, Khizar Ahmed, Prakash S. Dabeer, and Sher Afghan Khan. "Influence of expansion level on base pressure and reattachment length." *CFD Letters* 11, no. 5 (2019): 22-36.

[8] Azami, Muhammed Hanafi, Mohammed Faheem, Abdul Aabid, Imran Mokashi, and Sher Afghan Khan. "Inspection of supersonic flows in a CD nozzle using experimental method." *International Journal of Recent Technology and Engineering* 8, no. 2S3 (2019): 996-999. https://doi.org/10.35940/ijrte.B1186.0782S319

[9] Azami, Muhammed Hanafi, Mohammed Faheem, Abdul Aabid, Imran Mokashi, and Sher Afghan Khan. "Experimental research of wall pressure distribution and effect of micro jet at Mach 1.5." *International Journal of Recent Technology and Engineering* 8, no. 2S3 (2019): 1000-1003. https://doi.org/10.35940/ijrte.B1187.0782S319

[10] Pathan, Khizar Ahmed, Zakir Ilahi Chaudhary, Ajaj Rashid Attar, Sher Afghan Khan, and Ambareen Khan. "Optimization of Nozzle Design for Weight Reduction using Variable Wall Thickness." *Journal of Advanced Research in Fluid Mechanics and Thermal Sciences* 112, no. 2 (2023): 86-101. https://doi.org/10.37934/arfmts.112.2.86101

[11] Khan, Sher Afghan, Abdul Aabid, and Ahamed Saleel Chandu Veetil. "Influence of micro-jets on the flow development in the enlarged duct at supersonic Mach number." *International Journal of Mechanical and Mechatronics Engineering* 19, no. 1 (2019): 70-82.

[12] Khan, Sher Afghan, and E. Rathakrishnan. "Active control of suddenly expanded flows from under-expanded nozzles-Part II." *International Journal of Turbo and Jet Engines* 22, no. 3 (2005): 163-184. https://doi.org/10.1515/TJJ.2005.22.3.163

[13] Khan, Sher Afghan, M. A. Fatepurwala, and K. N. Pathan. "CFD analysis of human-powered submarine to minimize drag." *International Journal of Mechanical and Production Engineering Research and Development (IJMPERD)* 8, no. 3 (2018): 1057-1066. https://doi.org/10.24247/ijmperdjun2018111

[14] Pathan, Khizar A., Sher A. Khan, N. A. Shaikh, Arsalan A. Pathan, and Shahnawaz A. Khan. "An investigation of boattail helmet to reduce drag." *Advances in Aircraft and Spacecraft Science* 8, no. 3 (2021): 239.

[15] Fakhruddin, Ahmad 'Afy Ahmad, Fharukh Ahmed Ghasi Mahaboobali, Ambareen Khan, Mohammad Nishat Akhtar, Sher Afghan Khan, and Khizar Ahmad Pathan. "Analysis of Base Pressure Control with Ribs at Mach 1.2 using CFD Method." *Journal of Advanced Research in Fluid Mechanics and Thermal Sciences* 123, no. 1 (2024): 108-143. https://doi.org/10.37934/arfmts.123.1.108143

[16] Khan, Ambareen, Parvathy Rajendran, Junior Sarjit Singh Sidhu, S. Thanigaiarasu, Vijayanandh Raja, and Qasem Al-Mdallal. "Convolutional neural network modeling and response surface analysis of compressible flow at sonic and supersonic Mach numbers." *Alexandria Engineering Journal* 65 (2023): 997-1029. https://doi.org/10.1016/j.aej.2022.10.006

[17] Khan, Ambareen, Parvathy Rajendran, Junior Sarjit Singh Sidhu, and Mohsen Sharifpur. "Experimental investigation of suddenly expanded flow at sonic and supersonic Mach numbers using semi-circular ribs: a comparative study between experimental, single layer, deep neural network (SLNN and DNN) models." *The European Physical Journal Plus* 138, no. 4 (2023): 314. https://doi.org/10.1140/epjp/s13360-023-03853-1

[18] Shaikh, Javed S., Krishna Kumar, Khizar A. Pathan, and Sher A. Khan. "Analytical and computational analysis of pressure at the nose of a 2D wedge in high-speed flow." *Advances in Aircraft and Spacecraft Science* 9, no. 2 (2022): 119-130.

[19] Shamitha, Shamitha, Asha Crasta, Khizer Ahmed Pathan, and Sher Afghan Khan. "Numerical simulation of surface pressure of a wedge at supersonic Mach numbers and application of design of experiments." *Journal of Advanced Research in Applied Mechanics* 101, no. 1 (2023): 1-18. https://doi.org/10.37934/aram.101.1.118

[20] Shamitha, Shamitha, Asha Crasta, Khizar Ahmed Pathan, and Sher Afghan Khan. "Analytical and Numerical Simulation of Surface Pressure of an Oscillating Wedge at Hypersonic Mach Numbers and Application of Taguchi's

Method." *Journal of Advanced Research in Applied Sciences and Engineering Technology* 30, no. 1 (2023): 15-30. https://doi.org/10.37934/araset.30.1.1530

[21] Shaikh, Javed Shoukat, Khizar Ahmed Pathan, Krishna Kumar, and Sher Afghan Khan. "Effectiveness of Cone Angle on Surface Pressure Distribution along Slant Length of a Cone at Hypersonic Mach Numbers." *Journal of Advanced Research in Fluid Mechanics and Thermal Sciences* 104, no. 1 (2023): 185-203. https://doi.org/10.37934/arfmts.104.1.185203

[22] Shaikh, Javed S., Krishna Kumar, Khizar A. Pathan, and Sher A. Khan. "Computational analysis of surface pressure distribution over a 2D wedge in the supersonic and hypersonic flow regimes." *Fluid Dynamics & Materials Processing* 19, no. 6 (2023). https://doi.org/10.32604/fdmp.2023.025113

[23] Chaudhari, Pavan Bhaskar, Rachayya Arakerimath, Khizar Ahmed Pathan, and Sher Afghan Khan. "Comparative Experimental Analysis and Performance Optimization of Single-Cylinder DI and HCCI Engine with Series Catalytic Converters." *Journal of Advanced Research in Fluid Mechanics and Thermal Sciences* 121, no. 1 (2024): 173-187. https://doi.org/10.37934/arfmts.121.1.173187

[24] Jain, Yogeshkumar, Vijay Kurkute, Sagar Mane Deshmukh, Khizar Ahmed Pathan, Ajaj Rashid Attar, and Sher Afghan Khan. "The Influence of Plate Fin Heat Sink Orientation under Natural Convection on Thermal Performance: An Experimental and Numerical Study." *Journal of Advanced Research in Fluid Mechanics and Thermal Sciences* 114, no. 2 (2024): 118-129. https://doi.org/10.37934/arfmts.114.2.118129

[25] Khalil, Shaikh Sohel Mohd, Rai Sujit Nath Sahai, Nitin Parashram Gulhane, Khizar Ahmed Pathan, Ajaj Rashid Attar, and Sher Afghan Khan. "Experimental Investigation of Local Nusselt Profile Dissemination to Augment Heat Transfer under Air Jet Infringements for Industrial Applications." *Journal of Advanced Research in Fluid Mechanics and Thermal Sciences* 112, no. 2 (2023): 161-173. https://doi.org/10.37934/arfmts.112.2.161173

[26] Shaikh, Sohel Khalil, Khizar Ahmed Pathan, Zakir Ilahi Chaudhary, B. G. Marlpalle, and Sher Afghan Khan. "An investigation of three-way catalytic converter for various inlet cone angles using CFD." *CFD Letters* 12, no. 9 (2020): 76-90. https://doi.org/10.37934/cfdl.12.9.7690

[27] Shaikh, Sohel Khalil, Khizar Ahmed Pathan, Zakir Ilahi Chaudhary, and Sher Afghan Khan. "CFD analysis of an automobile catalytic converter to obtain flow uniformity and to minimize pressure drop across the monolith." *CFD Letters* 12, no. 9 (2020): 116-128. https://doi.org/10.37934/cfdl.12.9.116128

[28] Kale, Dipak, Rachayya Arakerimath, Khizar Ahmed Pathan, and Sher Afghan Khan. "Investigation on Water Erosion Behavior of Ti-based Metal Matrix Composite: Experimental Approach." *Journal of Advanced Research in Fluid Mechanics and Thermal Sciences* 122, no. 2 (2024): 71-82. https://doi.org/10.37934/arfmts.122.2.7182

[29] Sheikh, Fahim Rahim, Suresh Pandurang Deshmukh, Purushottam Ardhapurkar, Khizar Ahmed Pathan, Sohel Khalil Shaikh, and Sher Afghan Khan. "Modeling and Experimental Validation of NePCM-Nanofluid-Based PVT System." *Journal of Advanced Research in Fluid Mechanics and Thermal Sciences* 122, no. 1 (2024): 205-222. https://doi.org/10.37934/arfmts.122.1.205222

[30] Khan, Ambareen, Abdul Aabid, Sher Afghan Khan, Mohammad Nishat Akhtar, and Muneer Baig. "Comprehensive CFD analysis of base pressure control using quarter ribs in sudden expansion duct at sonic Mach numbers." *International Journal of Thermofluids* 24 (2024): 100908. https://doi.org/10.1016/j.ijft.2024.100908

[31] Khan, Ambareen, Sher Afghan Khan, Vijayanandh Raja, Abdul Aabid, and Muneer Baig. "Effect of ribs in a suddenly expanded flow at sonic Mach number." *Heliyon* 10, no. 9 (2024). https://doi.org/10.1016/j.heliyon.2024.e30313

[32] Khan, Ambareen, Sher Afghan Khan, Mohammed Nishat Akhtar, Abdul Aabid, and Muneer Baig. "Base Pressure Control with Semi-Circular Ribs at Critical Mach Number." *Fluid Dynamics & Materials Processing* 20, no. 9 (2024). https://doi.org/10.32604/fdmp.2024.049368

[33] Nurhanis, Tun, Ambareen Khan, Mohammad Nishat Akhtar, and Sher Afghan Khan. "Control of Base Pressure at Supersonic Mach Number in a Suddenly Expanded Flow." *Journal of Advanced Research in Fluid Mechanics and Thermal Sciences* 109, no. 1 (2023): 210-225. https://doi.org/10.37934/arfmts.109.1.210225

[34] Khan, Ambareen, Nurul Musfirah Mazlan, and Mohd Azmi Ismail. "Velocity Distribution and Base Pressure Analysis of Under Expanded Nozzle Flow at Mach 1.0." *Journal of Advanced Research in Fluid Mechanics and Thermal Sciences* 92, no. 1 (2022): 177-189. https://doi.org/10.37934/arfmts.92.1.177189

[35] Khan, Ambareen, Nurul Musfirah Mazlan, and Ervin Sulaeman. "Effect of Ribs as Passive Control on Base Pressure at Sonic Mach Numbers." *CFD Letters* 14, no. 1 (2022): 140-151. https://doi.org/10.37934/cfdl.14.1.140151

[36] Khan, Ambareen, Mohd Azmi Ismail, and Nurul Musfirah Mazlan. "Numerical Simulation of Suddenly Expanded Flow from Converging Nozzle at Sonic Mach Number." In *Proceedings of International Conference of Aerospace and Mechanical Engineering 2019: AeroMech 2019*, 20-21 November 2019, Universiti Sains Malaysia, Malaysia, pp. 349-359. Springer Singapore, 2020. https://doi.org/10.1007/978-981-15-4756-0_29

[37] Khan, Ambareen, Nurul Musfirah Mazlan, and Mohd Azmi Ismail. "Analysis of flow through a convergent nozzle at Sonic Mach Number for Area Ratio 4." *Journal of Advanced Research in Fluid Mechanics and Thermal Sciences* 62, no. 1 (2019): 66-79.

[38] Khan, Ambareen, Nurul Musfirah Mazlan, Mohd Azmi Ismail, and Mohammad Nishat Akhtar. "Experimental and numerical simulations at sonic and supersonic Mach numbers for area ratio 7.84." *CFD Letters* 11, no. 5 (2019): 50-60.

[39] Asadullah, Mohammed, Sher Afghan Khan, Waqar Asrar, and E. Sulaeman. "Low-cost base drag reduction technique." *International Journal of Mechanical Engineering and Robotics Research* 7, no. 4 (2018): 428-432. https://doi.org/10.18178/ijmerr.7.4.428-432

[40] Rathakrishnan, E. "Effect of ribs on suddenly expanded flows." *AIAA Journal* 39, no. 7 (2001): 1402-1404. https://doi.org/10.2514/2.1461